Original Research Article

Linking Methane Emissions to Iron Dynamics in Bioturbated Rice Systems

Qianrui Huangfu[1,2,a], Sha Zhang[1,2,a,*], Zheng Chen[3*], Lu Wang[1,2], Dong Zhu[1,2]

1 Key Laboratory of Urban Environment and Health, Ningbo Urban Environment Observation and Research Station, Institute of Urban Environment, Chinese Academy of Sciences, Xiamen 361021, China

2 Zhejiang Key Laboratory of Urban Environmental Processes and Pollution Control, Chinese Academy of Sciences Haixi Industrial Technology Innovation Center in Beilun, Ningbo 315830, China

3 Department of Health and Environmental Sciences, Xi'an Jiaotong-Liverpool University, 111 Ren'ai Road, Suzhou, Jiangsu, 215123, China

[a]The authors contribute equally.

*Corresponding authors

Lead contact:

Sha Zhang

Tel: +86-17798590069

Email: biogeochemx@outlook.com, szhang@iue.ac.cn

Address: Ningbo Observation and Research Station
Institute of Urban Environment, Chinese Academy of Sciences
No. 88 Zhongke Road, Chunxiao Street
Beilun District, Ningbo City
Zhejiang Province, China
Postal Code: 315800

Abstract

Iron (Fe) redox cycling is intricately linked to methane (CH_4) emissions in global wetlands, yet its role under sustained bioturbation remains poorly quantified. We investigated how continuous loach (*Misgurnus anguillicaudatus*) activity influences CH_4 emissions and Fe dynamics in a ratoon rice system over 178 days. Methane and ecosystem CO_2 fluxes were measured continuously, while in situ microdialysis quantified dissolved Fe in surface and root-zone porewaters. The results showed that loach bioturbation increased cumulative CH_4 emissions by 31.9% (95% CI: [18.2%, 40.2%], p = 0.0033) and sustained elevated dissolved Fe concentrations near the soil–water interface (SWI), indicating intensified reducing conditions and a weakened SWI barrier for CH_4. A Fe-based process model alone explained >78% of CH_4 flux variability. A more integrated model further suggested that loach activity enhanced CH_4 emissions by increasing labile carbon supply, CH_4 production efficiency, and CH_4 transport. These findings position dissolved Fe as a practical proxy for CH_4 emissions, with implications on improving global CH_4 models.

Keywords: Bioturbation; methane; microdialysis; oxic-anoxic interface; dissolved iron; ratoon (semi-perennial) rice; temperature sensitivity

Graphical abstract

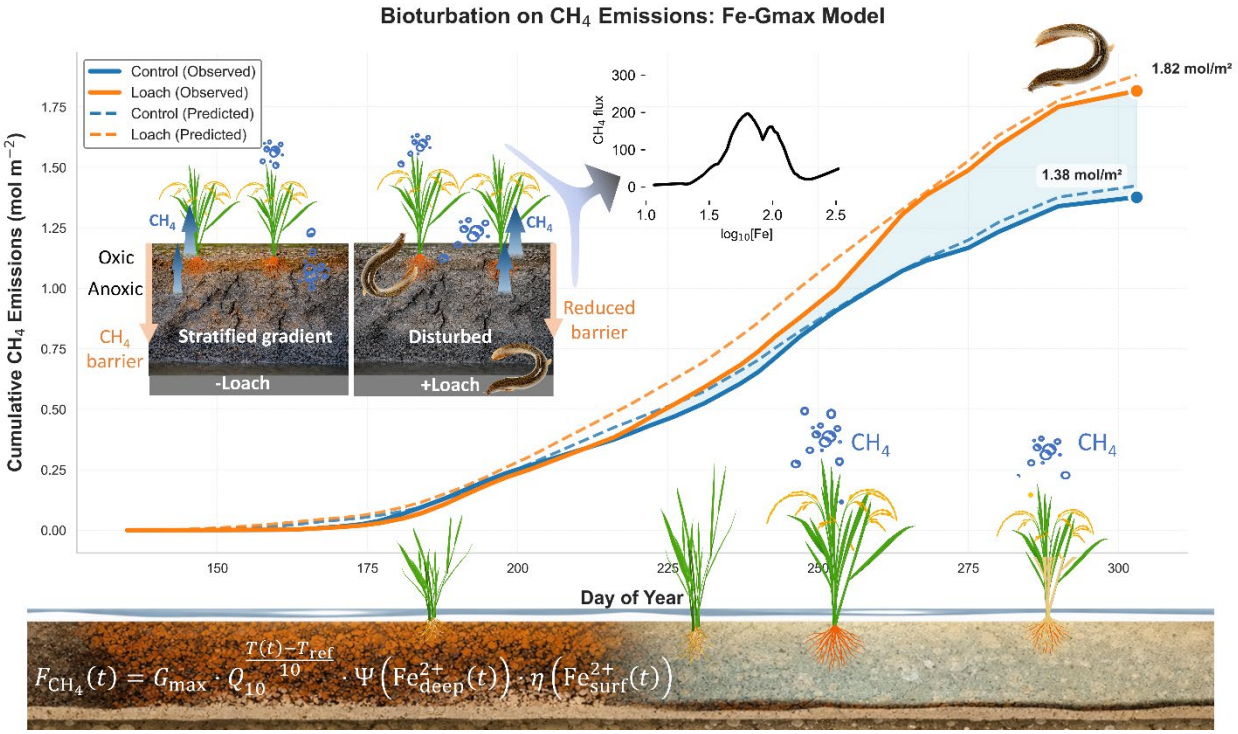

Highlights

- Stratified microdialysis revealed increased surface ferric reduction.
- Loach activity increased cumulative CH_4 emissions by 31.9% over 178d rice season.
- Seasonal CH_4 was positively linked to bottom Fe and negatively to surface Fe.
- Temperature regulated CH_4 indirectly via CO_2 fluxes and rice phenological stages.
- Surface dissolved Fe emerged as a practical proxy for seasonal CH_4 emissions.

Introduction

Biogeochemical cycles are fundamentally driven by perturbations that reorganize redox gradients and substrate availability across Earth's critical zone [1-4]. Among these, biological disturbances—from microbial metabolism to macrofaunal bioturbation—exert primary control on greenhouse gas (GHG) fluxes by mediating electron acceptor competition and carbon transformation pathways [5, 6]. Flooded agroecosystems like rice paddies, contributing ~8-12% of global anthropogenic CH_4 emissions (~30 Tg CH_4 yr^{-1}) [3, 6], represent highly dynamic systems in which redox processes, plant physiology, and biological disturbance interact to shape CH_4 cycling [5, 7, 8].

Under flooded conditions, CH_4 production, oxidation, and emission are not uniformly distributed throughout the soil profile but are constrained by **two critical redox interfaces**: the **soil–water interface (SWI)** and the **rhizosphere** [3, 9, 10]. Microorganisms at the SWI can oxidize > 40% of CH_4 [3]. The rhizosphere oxygen release forms localized oxidized microsites that regulate CH_4 production, oxidation, and plant-mediated transport [11]. The integrity and oxidative capacity of these two interfaces largely determine whether CH_4 is retained and oxidized within flooded soils or rapidly released to the atmosphere.

Bioturbation profoundly alters the structure and functioning of these interfaces, yet its net effect on CH_4 emissions remains unresolved. Numerous studies report reduced CH_4 emissions under bioturbated conditions [5, 12-14] due to enhanced oxygen penetration and stimulated oxidative processes at interfacial zones [3, 15-17]. In contrast, sustained benthic activities such as loaches, shrimp or *Paphia undulata* can increase CH_4 emissions by accelerating organic matter mineralization, increasing labile carbon availability, and disrupting redox stability [18-23]. These contrasting outcomes suggest that the presence of bioturbation alone is insufficient to predict CH_4 responses; rather, **the key lies in how bioturbation reshapes redox processes at interface scales**.

Mechanistic understanding of these effects is further constrained by methodological limitations. In field settings, spatial heterogeneity of animal activity, external feed inputs, and variable water management complicate isolation of bioturbation effects [5, 8, 18, 19, 24]. Low-frequency CH_4 measurements may miss emission peaks [3], fixed-point measurements may not confirm active bioturbation [25, 26], and most studies focus on single growing seasons, implicitly assuming post-harvest reoxidation. Such assumptions overlook the persistence of reduced conditions and root biomass in semi-perennial (or ratoon) rice systems [27]. Critically, **there remains a lack of process-based indicators that can quantitatively link interfacial redox dynamics to CH_4 fluxes under sustained bioturbation**.

The identification of a mechanistically meaningful and operationally **robust indicator** is essential (Fig. 1). Bulk redox potential (Eh) integrates multiple processes and lacks specificity, while field measurements often show poor reproducibility [28]. Dissolved oxygen is extremely low and highly transient under flooded conditions, and alternative electron acceptors such as nitrate or sulfate exhibit rapid turnover and limited inventories, restricting their relevance to short temporal windows. In contrast, iron (Fe) is abundant in flooded soils and undergoes continuous redox cycling between Fe(III) and Fe(II) across relevant spatial and temporal scales [4, 29], during which **Fe reduction consume about 50% e-donors** [30, 31]. Microbial Fe(III) reduction directly competes with methanogenesis for electron donors and can be coupled to anaerobic CH_4 oxidation, whereas reoxidation of Fe(II) at the SWI and in the rhizosphere reinforces oxidative barrier functions at both interfaces [3, 32]. Because Fe redox cycling is intrinsically coupled to CH_4-related processes and integrates cumulative redox information across interfaces and time, Fe represents the most plausible proxy for establishing quantitative linkages to CH_4 emissions in flooded systems [33, 34]. **Despite this potential, direct evidence linking depth-resolved Fe redox dynamics to CH_4 emissions under sustained bioturbation remains scarce**.

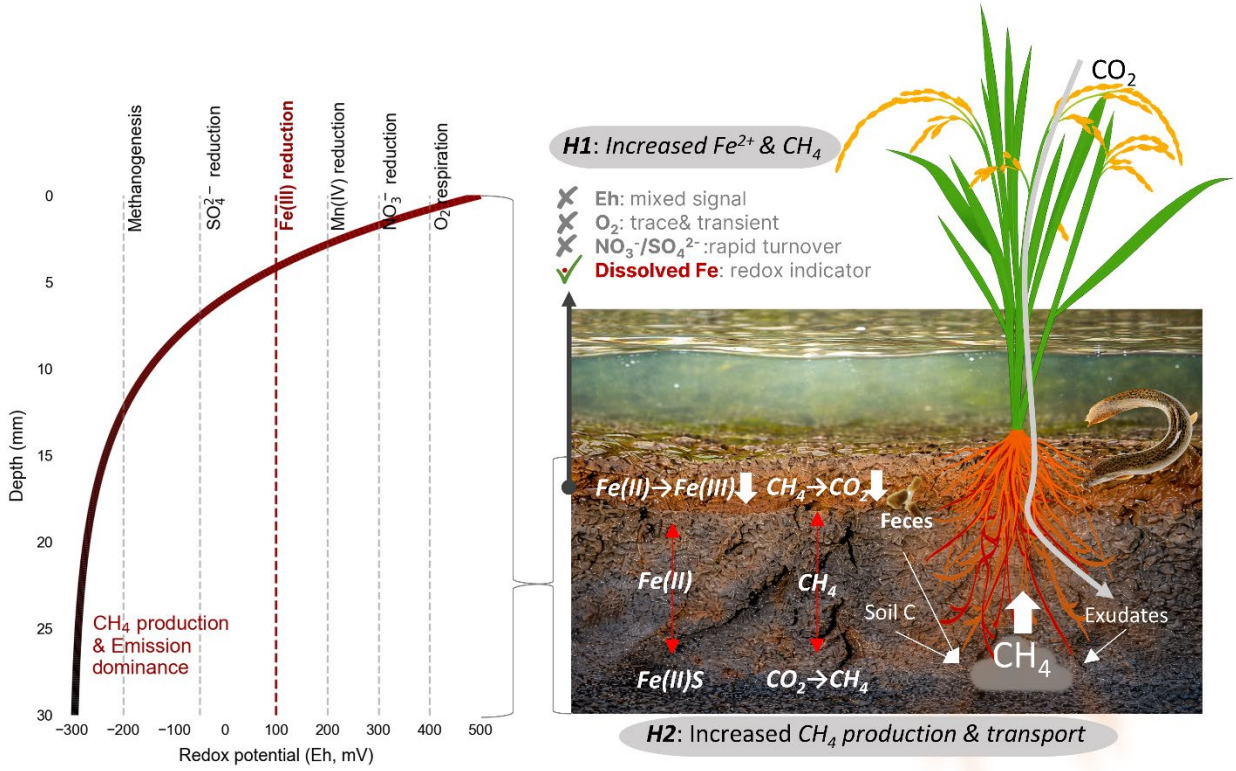

Fig. 1. Hypothesized role of dissolved Fe as an integrated redox indicator of bioturbation-mediated CH_4 emissions in flooded rice systems. Methane produced in anoxic soils must traverse an oxidized Fe belt at the SWI, with possible extension to floating Fe biofilms at the water–air interface and root Fe plaques. Fish

bioturbation increases labile carbon inputs and disrupts the SWI CH_4 barrier, enhancing Fe reduction, CH_4 production, and emissions, forming the basis of hypotheses H1 and H2.

We tried to address these gaps through a 178-day mesocosm experiment integrating ratoon rice with benthic loaches (*Misgurnus anguillicaudatus*) under feed-free conditions. Continuous CH_4/CO_2 flux monitoring, in situ microdialysis of porewater Fe at surface/root-zone depths, and process-based modeling tested two hypotheses (Fig. 1): (1) Loach bioturbation weakens SWI barrier function, elevating surface soil reducing conditions; (2) Dissolved Fe serves as a robust CH_4 emission proxy across seasonal scales. By establishing Fe redox as a mechanistic integrator of bioturbation effects, this study provides quantitative constraints for global CH_4 models and allows simulating the net impact of bioturbation in flooded systems.

2. Materials and Methods

2.1. Soil location and characterization

Paddy soil collected from Shangyu City (30°01’38.256” N, 120°52’23.311” E), Zhejiang in China, characterized by total organic matter (3.5% by weight), with a soil paste pH of 5.6, 3.5% Fe and loam characteristics. Other soil properties were described previously [35].

2.2. Open-field rice growth experiment

An open field mesocosm experiment was conducted to examine the effects of loach bioturbation on rice growth and GHG fluxes. The experiment included two treatments: rice grown without loach (−Loach) and rice grown with loach (+Loach), each with two replicate soil containers.

The experimental units consisted of polyvinyl chloride (PVC) container tanks (30 × 40 cm, length × width), each filled with approximately 20 kg of sieved air-dried soil. On day of year (DOY) 167, two loaches (*Misgurnus anguillicaudatus*) were introduced into each +Loach container, whereas −Loach containers received no loach fishes. Prior to introduction, loaches were pre-cultured under natural rainwater conditions for approximately 30 days and sustained by aquatic plants and duckweeds transplanted from the experimental soil. Throughout the rice–loach cocultivation period, loaches foraged on naturally available food sources, including soil organic matter, snails, *Alligator weed*, *Cyperus difformis*, macroalgae, phytoplankton, and other zoobenthos and zooplankton [18].

Basal nitrogen fertilizer was applied as urea at a rate equivalent to 60 kg N ha^{-1} at the beginning of the growing season. No additional organic amendments were applied during the experiment. Seeds of the rice cultivar *Yliangyou No.1* were germinated in deionized water and raised for four weeks on a horticultural substrate. Subsequently, six rice hills consisting of 25-day-old seedlings were uniformly transplanted into each container.

All containers were embedded in a large sand bed filled with river sand, with a total sand volume at least 20 times greater than the combined volume of the containers. This configuration ensured continuous submergence of the containers and insulated the sidewalls from direct solar radiation. The sand bed was maintained under flooded conditions, producing a stable water column of approximately 5 cm above the soil surface in each container. This design minimizes edge effects and temperature heterogeneity associated with uneven heating. To maintain consistent flooding throughout the experimental period, a rainwater collection system was used to compensate for evaporative water losses, thereby supporting a near-natural hydrological regime under open-field conditions. In addition, thermocouples were installed at a soil depth of 5–10 cm. Temperature was recorded at 30-min intervals using a remote temperature monitoring data logger (Xiandun CIMC Inc., China) [27].

2.3. Chamber-based CH_4 flux measurement

Methane and CO_2 fluxes were measured at intervals of 3–10 days using a static half-transparent chamber approach coupled with a portable greenhouse gas analyzer (LI-7810, LI-COR Biosciences). During each measurement, the analyzer continuously recorded CH_4 and CO_2 concentrations following chamber closure [3, 36]. Gas fluxes were calculated based on the initial rate of change in gas mole fraction (∂C/∂t) according to Equation (1):

$$J = \frac{\partial C_{CH_4}}{\partial t} \times \frac{V}{A} \times \frac{P(1-W_0)}{RT} \quad (1)$$

where J is the gas flux (μmol m^{-2} s^{-1}), V is the chamber volume (0.1925 m^3), A is the soil surface area enclosed by the chamber (0.12 m^2), P is atmospheric pressure (101.3 kPa), W_o is the mean water vapor mole fraction during each measurement, R is the universal gas constant (0.008134 m^3 kPa mol^{-1} K^{-1}), and T is soil temperature (K) measured at 5 cm depth. The term $\frac{\partial C_{CH_4}}{\partial t}$ represents the rate of change in gas mole fraction (μmol mol^{-1} s^{-1}) immediately after chamber closure. Carbon dioxide fluxes were measured in the similar way. These measurements represent instantaneous net ecosystem exchange (NEE), integrating both photosynthetic CO_2 uptake and respiratory CO_2 release within the chamber.

To resolve short-term dynamics, intensive flux measurements were conducted during the grain-filling stage of the main rice crop. On day of year (DOY) 242, gas fluxes were measured every 1–2 hours throughout the daytime to capture diurnal variability and its relationships with environmental drivers, including air temperature and soil temperature.

The gas analyzer was automatically calibrated using standard gas mixtures prior to measurements. Air samples were partially dehydrated using an integrated gas dryer before entering the analyzer. During each measurement, real-time changes in CH_4, CO_2, and H_2O concentrations were monitored to identify disturbances caused by abrupt

perturbations or gas ebullition. Measurements showing irregular concentration changes were discarded and repeated. Flux calculations were based on the initial linear concentration change beginning 30 s after chamber closure.

Linear regression coefficients were recorded for each measurement, and all raw concentration data were archived for quality control. Flux estimates were accepted only when the coefficient of determination (R^2) exceeded 0.75 and the root mean square error (RMSE) was below 1.5% for CO_2 (300–700 ppm) or below 2 ppb for CH_4. During gas flux measurements, concurrent environmental variables were monitored, including soil temperature at 5 cm depth, canopy air temperature, relative humidity, and photosynthetic photon flux density (PPFD), using an on-site miniature weather station.

2.4. Soil microdialysis and dissolved Fe analysis

Soil porewater redox dynamics were investigated using in situ soil microdialysis, following the methodological framework established in previous studies [9, 10]. Microdialysis sampling was conducted repeatedly throughout the experimental period, with increased frequency during key rice growth stages. Microdialysis probes were installed at two soil depths: near the soil surface (covered only by the device) and at approximately 5–10 cm depth, allowing simultaneous monitoring of redox dynamics in both layers. Dialysate samples were pipetted into acid-cleaned polypropylene vials, and collected volumes were recorded for concentration calculations.

Immediately after collection, dialysate samples were acidified to pH < 2 with ultrapure nitric acid to stabilize dissolved Fe species. Dissolved Fe concentrations were quantified using inductively coupled plasma mass spectrometry (ICP-MS). Instrument calibration was performed using multi-element standard solutions, and procedural blanks were included to ensure analytical accuracy. Quality control was assessed through repeated analysis of standards and selected samples. Microdialysis-derived dissolved Fe concentrations were used to characterize soil redox status and redox succession rather than to directly quantify microbial Fe reduction rates.

2.5. Conceptual and mathematical framework of Fe–CH_4 coupling

Here, we formalize the conceptual understanding of Fe–carbon interactions in flooded soils into a minimal, process-based mathematical framework that links Fe redox dynamics to CH_4 production and CH_4 emission efficiency (More details in TEXT S1).

2.5.1 Thermodynamic hierarchy of redox processes

The framework is grounded in the thermodynamic hierarchy of anaerobic respiration in flooded soils, in which terminal electron-accepting processes proceed sequentially from Fe(III) reduction to sulfate reduction and ultimately to methanogenesis [16, 37, 38]. Ferric oxides consume more than 50% electron donors in freshwater environment [30]. As long as reactive Fe(III) remains available, Fe reduction competitively consumes shared electron donors and suppresses CH_4 production [33]. Methanogenesis is assumed to initiate only after Fe(III) becomes depleted or kinetically constrained, and deep-layer Fe^{2+} is subsequently immobilized through sulfide precipitation. A more reducing environment would result in a lower dissolved Fe concentration.

2.5.2 Dual role of Fe in regulating CH_4 dynamics

Iron is assumed to regulate CH_4 cycling through two distinct but interconnected mechanisms operating at different soil depths. In deeper soil layers, reactive Fe(III) indirectly controls CH_4 production by scavenging sulfide and alleviating sulfate inhibition, thereby shaping the timing and magnitude of CH_4 generation. In contrast, in surface soil layers, Fe redox cycling directly governs CH_4 oxidation. Oxidized Fe phases serve as electron acceptors for CH_4 oxidation, whereas elevated Fe^{2+} concentrations indicate increasingly reducing conditions that weaken oxidative capacity. These contrasting controls motivate a vertically stratified representation of the soil system (section 2.4).

2.5.3 Spatial compartmentalization and process coupling

The soil profile is conceptualized as two functionally distinct compartments: a deep methanogenic zone and a surface oxidative layer. Methane production is assumed to occur predominantly in deeper soil layers, whereas CH_4 oxidation and transport regulation are controlled near the SWI. Although these processes are modeled independently, they are coupled through CH_4 diffusion, such that variations in deep CH_4 production propagate upward to influence surface emission efficiency.

2.5.4 Functional representation of CH_4 production

Methane production potential in the deep soil layer is assumed to depend nonlinearly on dissolved Fe^{2+} concentration. High Fe^{2+} concentrations indicate active Fe reduction and strong suppression of methanogenesis. As Fe^{2+} is progressively removed through sulfide fixation, this suppression is relaxed, resulting in a rapid increase in CH_4 production potential. This transition is represented using an inverse sigmoidal function:

$$\Psi\left(\mathrm{Fe}^{2+}_{\mathrm{deep}}\right) = \left(1 - \frac{\mathrm{Fe}^{2+}_{\mathrm{deep}}}{\mathrm{Fe}^{2+}_{\mathrm{deep}} + K_{\mathrm{trig}}}\right)^{m} \quad (1)$$

where K_{trig} denotes the Fe^{2+} concentration at which methanogenesis is half-released from Fe-mediated suppression, and m controls the sharpness of the transition.

2.5.5 Functional representation of CH_4 oxidation efficiency

Methane oxidation efficiency in the surface layer is assumed to decline monotonically with increasing Fe^{2+} concentration, reflecting a shift toward more reducing conditions and diminished oxidative capacity. This behavior is described using a Hill-type function:

$$\eta\left(\mathrm{Fe}^{2+}_{\mathrm{surf}}\right) = \eta_0 + (1 - \eta_0) \cdot \frac{\left(\mathrm{Fe}^{2+}_{\mathrm{surf}}\right)^{p}}{K^{p}_{\mathrm{emit}} + \left(\mathrm{Fe}^{2+}_{\mathrm{surf}}\right)^{p}} \quad (2)$$

where η_0 represents the minimum oxidation efficiency under strongly reducing conditions, K_{emit} defines the Fe^{2+} concentration at which oxidation efficiency is reduced by half, and p controls the sensitivity of the response.

2.5.6 Temperature response and process decoupling

Temperature effects on CH_4 production are represented using a Q_{10} formulation, assuming constant temperature sensitivity across the studied range:

$$f(T) = Q_{10}^{\frac{T - T_{\mathrm{ref}}}{10}} \quad (4)$$

2.5.7 Parameterization of maximum CH_4 production capacity (G_{max})

The maximum CH_4 production capacity (G_{max}) represents the upper limit of substrate-supported methanogenesis under optimal redox and temperature conditions. Rather than treating G_{max} as a purely empirical constant, we parameterized it as a dynamic quantity linked to carbon input availability, reflecting

the coupling between plant-derived carbon supply, additional organic inputs, and microbial CH_4 production potential.

Specifically, $G_{\max}$was decomposed into a baseline carbon input term modulated by photosynthetic activity and, where applicable, an additional organic carbon contribution associated with animal-derived inputs. Photosynthetic activity was inferred from net CO_2 fluxes and translated into a photosynthesis potential index, accounting for the fact that enhanced respiration in bioturbated systems may obscure gross carbon assimilation when only net CO_2 exchange is observed. To reflect delayed carbon translocation from aboveground production to belowground substrates, a temporal lag was introduced using an exponentially weighted moving average. ethane emissions exhibit a time-lagged response to key drivers such as temperature and plant productivity, as demonstrated by global analyses of the FLUXNET-CH4 dataset [39, 40].

For systems without animal inputs, $G_{\max}$ was expressed as a function of photosynthesis-modulated plant carbon input:

$$G_{\max}(t) = G_{\text{base}}\left[1 + k_{\text{photo}} \cdot \frac{P_{\text{lag}}(t) - P_{\text{ref}}}{P_{\text{ref}}}\right] \qquad (5a)$$

where $G_{\text{base}}$is the baseline CH_4 production capacity, k_{photo}quantifies the sensitivity of CH_4 production to photosynthetic carbon input, $P_{\text{lag}}(t)$denotes lagged photosynthesis potential, and $P_{\text{ref}}$is a reference level used for normalization.

In systems with benthic fauna, $G_{\max}$additionally incorporated an animal-derived organic carbon input term, representing fecal deposition and enhanced organic matter turnover induced by bioturbation. In this case, total CH_4 production capacity was formulated as:

$$G_{\max}(t) = \left[G_{\text{plant}}(t) + G_{\text{feces}}(t)\right] \cdot k_{\text{meth}} \qquad (5b)$$

where $G_{\text{plant}}(t)$follows Eq. (5a), $G_{\text{feces}}(t)$represents the time-dependent contribution of animal-derived carbon inputs, and $k_{\text{meth}}$is a dimensionless conversion factor describing the efficiency with which available carbon substrates are converted into CH_4. Differences in k_{meth}between treatments capture treatment-

specific constraints on methanogenic efficiency arising from redox disturbance, microbial competition, or altered substrate quality.

Together, this formulation allows $G_{\max}$to vary dynamically in response to carbon supply while remaining mechanistically interpretable, thereby linking aboveground carbon assimilation, bioturbation-induced organic inputs, and subsurface CH_4 production within a unified modeling framework.

CH_4 production and oxidation are assumed to be separable processes operating at different soil depths. Accordingly, total CH_4 emission flux is calculated as the product of temperature-modulated CH_4 production potential and surface emission efficiency:

$$F_{CH_4}(t) = G_{\max} \cdot Q_{10}^{\frac{T(t)-T_{\mathrm{ref}}}{10}} \cdot \Psi\left(\mathrm{Fe}^{2+}_{\mathrm{deep}}(t)\right) \cdot \eta\left(\mathrm{Fe}^{2+}_{\mathrm{surf}}(t)\right) \quad (6)$$

2.5.8. Model parameters and input variables

Model parameters: The parameters used in the Fe–CH_4 coupling model, together with their physical interpretations and typical ranges reported in flooded soil systems, are summarized in Table 1. Parameter values were either constrained by literature ranges or calibrated against observed CH_4 flux dynamics, ensuring mechanistic interpretability rather than purely empirical fitting.

Table 1. Model parameters, symbols, physical meaning, and typical ranges.

Parameter	Symbol	Unit	Physical meaning	Typical range
Maximum production capacity	$G_{\max}$	nmol m^{-2} s^{-1}	Maximum CH_4 production potential under optimal redox and temperature conditions	1–1000 [39]
Deep-layer trigger threshold	K_{trig}	dimensionless	Threshold Fe^{2+} concentration controlling the release of Fe-mediated suppression on methanogenesis	10–700 [4]
Deep-layer shape parameter	m	dimensionless	Steepness of the deep-layer CH_4 production response to Fe^{2+} decline	0.5–5 (Empirically)
Minimum emission efficiency	η_0	dimensionless	Residual CH_4 emission efficiency under strongly oxidizing surface conditions	0.01–0.5 [33]
Surface half-saturation constant	K_{emit}	dimensionless	Fe^{2+} concentration at which surface emission efficiency reaches its midpoint	5–50 [34]
Surface shape parameter	p	dimensionless	Sensitivity of surface emission efficiency to Fe^{2+} variation	0.5–5 [34]
Temperature sensitivity	Q_{10}	dimensionless	Multiplicative increase in reaction rate for a 10 °C rise in temperature	1.5–4.0 [41]

Input variables: The model is driven by time-resolved environmental and biogeochemical input variables (Table 2). Dissolved Fe^{2+} concentrations in deep and surface soil layers represent the redox state of the methanogenic and oxidative compartments, respectively. Soil temperature regulates CH_4 production through a Q_{10}-type response, while CO_2 flux is used as a proxy for ecosystem carbon exchange and photosynthetic activity in the parameterization of $G_{\max}$.

Table 2. Model input variables and descriptions.

Variable	Symbol	Unit	Description
Time	t(DOY)	day	Day of year
Deep-layer dissolved Fe	$\mathrm{Fe}^{2+}_{\mathrm{deep}}(t)$	dimensionless	Relative total dissolved Fe concentration in the deep, methanogenic soil layer
Surface-layer dissolved Fe	$\mathrm{Fe}^{2+}_{\mathrm{surf}}(t)$	dimensionless	Relative total dissolved Fe concentration in the surface, oxidative soil layer
Soil temperature	$T(t)$	°C	Time series of soil temperature
Reference temperature	T_{ref}	°C	Reference temperature for the Q_{10} response (default: 25 °C)
Net CO_2 flux	$F_{\mathrm{CO_2}}(t)$	μmol m^{-2} s^{-1}	Net ecosystem CO_2 exchange, used as a proxy for photosynthetic carbon input in the parameterization of $G_{\max}$

Net CO_2 flux was incorporated to capture variations in plant-derived carbon supply that regulate CH_4 production capacity. Because net CO_2 exchange reflects the balance between photosynthesis and respiration, its influence on $G_{\max}$was interpreted in combination with temporal smoothing to account for delayed translocation of assimilated carbon to belowground substrates, as described in Section 2.5.7.

2.6. Statistical analysis

All analyses were conducted in Python 3.10 using numpy, pandas, scipy, and statsmodels. Results are reported as means ± standard deviations unless otherwise stated. For CH_4 flux data, differences between treatments (+Loach vs -Loach) were evaluated using paired t-tests across all sampling dates, with cumulative emission differences quantified using trapezoidal integration and uncertainty estimated via bootstrap resampling (n = 10,000 iterations). Treatment effects on seasonal or stage-averaged variables (e.g., greenhouse gas fluxes and porewater elemental concentrations) were assessed using two-tailed Student's *t*-tests (scipy.stats.ttest_ind). To avoid pseudoreplication, comparisons were based on values averaged over defined growth stages or measurement periods rather than individual observations. Fold changes were calculated to quantify relative differences between loach treatments and controls. For dissolved Fe concentrations after DOY 242, bottom-layer and surface-layer Fe were predicted using an XGBoost model

driven by environmental variables and gas fluxes, with hyperparameters tuned by cross-validation and uncertainty estimated via residual variance and quantile regression. Nonlinear relationships between dissolved Fe concentrations and CH_4 fluxes were examined using LOESS smoothing. Data from all treatments and soil layers were pooled, and Fe concentrations were $\log_{10}$-transformed prior to analysis. LOESS was implemented as robust local linear regression (it = 3) with the statsmodels LOWESS function, with the smoothing parameter selected by five-fold cross-validation. Resulting R^2 values are reported as descriptive indicators of fit, and uncertainty was estimated using bootstrap-derived 95% confidence intervals. Associations between CH_4 fluxes and environmental variables (air and soil temperature, relative humidity, vapor pressure deficit, and CO_2 flux) were evaluated using simple linear regressions (statsmodels.OLS). These analyses were intended to characterize treatment-specific response sensitivities rather than infer causality; slopes, R^2 values, and *p*-values are reported.

3. Results and discussion

3.1. Seasonal dynamics of CH_4/CO_2 fluxes and temperatures

At the seasonal scale, loach-rice co-cultivation significantly increased cumulative CH_4 emissions (Fig. 2a, b). Total CH_4 emissions in +Loach group were 29.06 ± 1.62 g m^{-2}, compared with 22.03 ± 0.91 g m^{-2} in -Loach group, representing a 31.9% (95% CI: [18.2%, 40.2%], $p = 0.0033$, Cohen's d = 0.510) increase. Most emissions occurred from main-season grain filling to ratoon stages, peaking after the first-season harvest. This period typically coincides with increased organic carbon inputs from senescing leaves.

Loach effects varied depending on environmental conditions. During early tillering (DOY 162–177), +Loach exhibited significantly lower CH_4 flux (-43.3% ± 9%, $p < 0.001$), during which turbid water and brown color (vs. grey color in -Loach group) of surface soil were observed, which suggested a more oxidized redox status. In contrast, during flowering to grain filling (DOY 202–226), CH_4 fluxes increased in loach plots (29.8% ± 7.2%, $p = 0.001$), coinciding with clearer water and greater plant biomass (Fig. 2c, d). During DOY 242–243 of the main crop rice (the grain filling), diel dynamics of CH_4 and CO_2 fluxes were continuously measured for confirming that loach cultivation increased mean CH_4 fluxes by 26.1% from 207.08 to 280.28 nmol m^{-2} s^{-1} (Fig. S1). However, on DOY 243 the effect of single point measurements only yielded 3.3% ± 36.5%(1σ) effect, which suggested an underestimation of the daily emission. Seasonal CH_4 fluxes were positively correlated with air and soil temperatures ($R^2 = 0.29$–0.39, $p < 0.001$) and negatively correlated with CO_2 fluxes ($R^2 = 0.18$–0.23, $p < 0.05$), with no significant relationships observed for PPFD, relative humidity, or VPD (Fig. S2). Temperature peaks preceded CH_4 emissions by 7–14 d (R^2 increased to 0.635–0.694, $p < 0.001$), while CO_2 fluxes lagged CH_4 emissions by 7–21 d (R^2 increased to 0.696–0.706, $p < 0.001$, Figs. S1, S3–S4); this lag

structure was further supported by high-frequency measurements on DOY 242–243 (**Fig. S1**). Consistent with this lag structure, lagged soil temperature showed significant linear correlation with CH_4 fluxes (coefficient r **increased from -0.608–0 to 0.494–0.833, Fig. S5**).

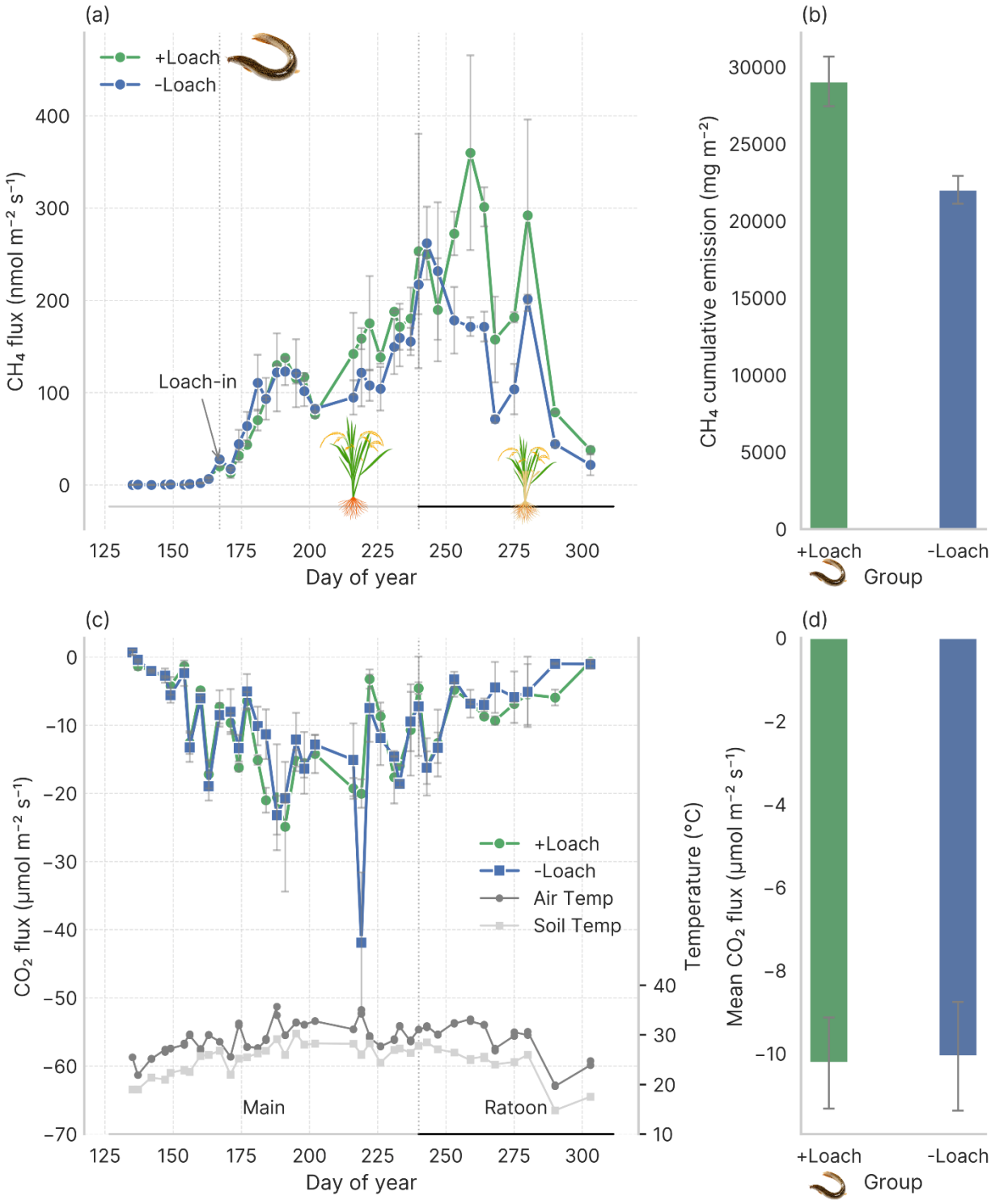

Fig. 2. Temporal dynamics of greenhouse gas fluxes, cumulative CH_4 emissions, seasonal mean CO_2 fluxes, and temperatures. (**a**, **b**) seasonal CH_4 flux (nmol m^{-2} s^{-1}) and cumulative CH_4 emissions (mg m^{-2}). (**c**, **d**) CO_2 flux (µmol m^{-2} s^{-1}) over time and mean CO_2 flux (µmol m^{-2} s^{-1}) across the measurement period. Each data point is shown as mean ± SD (n = 2-3). Air and soil temperatures during the flux measurement are presented in (c)

3.2 Dynamics of dissolved Fe concentrations at the SWI

Dissolved Fe concentrations showed strong depth stratification across the season, with deep-layer porewater (~5–8 cm) consistently exceeding surface concentrations (Fig. 3). At the first post-flooding sampling following rice transplanting, deep-layer Fe concentrations were already elevated, reaching 32.62 mg L^{-1} (+Loach) and 30.97 mg L^{-1} (−Loach). Note: Soils were flooded for months before soil wet mixing and transplanting. During the subsequent 25 days (seedling stage), deep-layer Fe increased rapidly to seasonal maxima of 279.08 mg L^{-1} (+Loach) and 330.46 mg L^{-1} (−Loach), before declining thereafter. Throughout this early phase, surface-layer Fe remained comparatively low and showed no consistent treatment differences.

Statistically significant treatment effects emerged within discrete temporal windows. During early-season periods (DOY 150–163 and 156–170), deep-layer porewater Fe concentrations were higher in the +Loach treatment (207.93 vs. 149.77 mg L^{-1}, t = 2.340, p = 0.0288; and 179.68 vs. 119.60 mg L^{-1}, t = 2.686, p = 0.0135; n = 12). In contrast, during the rice jointing stage (DOY 191–205 and 198–213), deep-layer Fe concentrations were significantly lower under +Loach conditions (99.00 vs. 111.97 mg L^{-1}, t = −3.359, p = 0.0028; and 85.86 vs. 94.16 mg L^{-1}, t = −2.607, p = 0.0167). Late in the season, treatment effects were primarily observed in surface-layer porewater, where +Loach exhibited consistently higher Fe concentrations across multiple windows (DOY 219–290, p < 0.001).

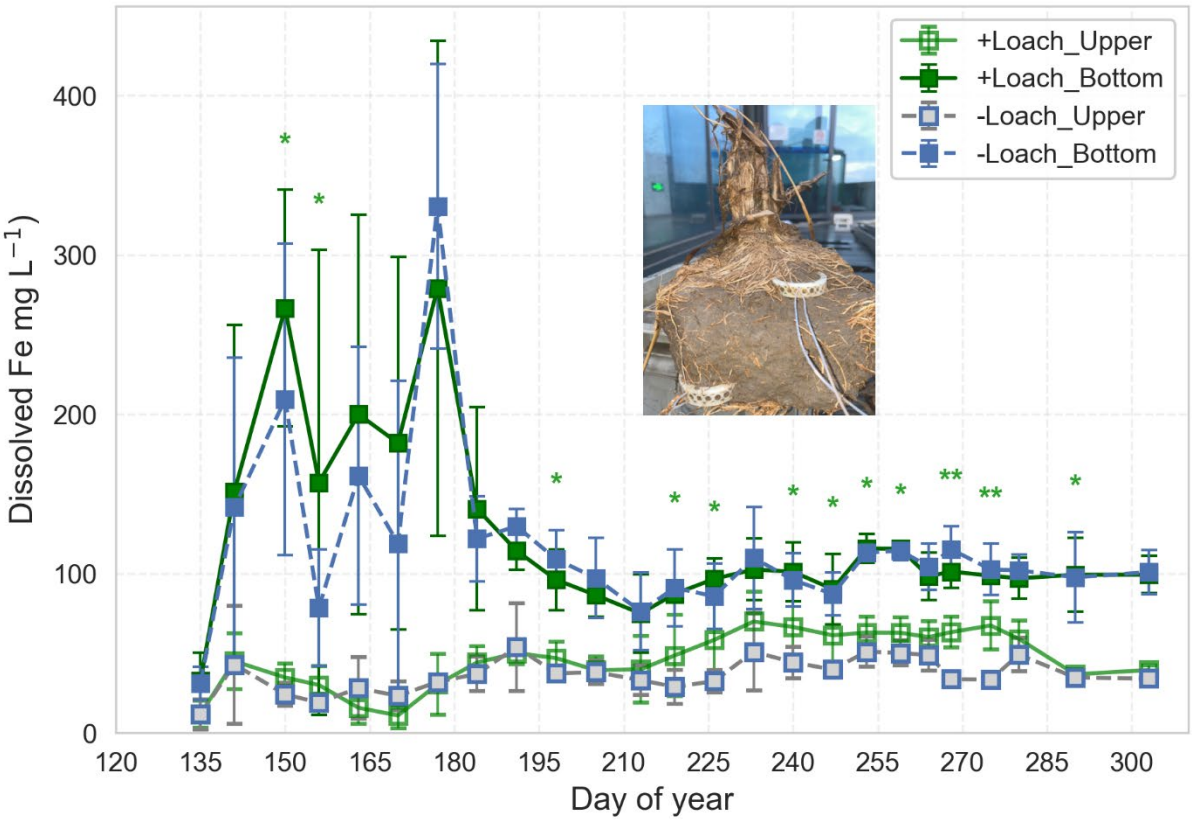

Fig. 3. Seasonal dynamics of dissolved Fe concentrations in the upper and bottom soil layers under fish-cultivated (+Loach) and control (−Loach) conditions during the flooded main and ratoon crop season. Data are shown as means ± std (n = 4 per time point) and plotted against DOY. The inserted photograph shows the location of the microdialysis device used for in situ porewater sampling. Asterisks (*) indicate significant differences between +Loach and −Loach treatments in the upper soil layer, while detail comparisons were summarized in Table S1.

3.4. The relationship between CH_4 fluxes and dissolved Fe concentrations

Across all observations, CH_4 flux exhibited a pronounced nonlinear relationship with dissolved Fe concentration, captured by LOESS smoothing (fraction = 0.2; Fig. 5, Fig. S4–S6), explaining 50.6% of the variance (R^2 = 0.506, n = 152, p < 0.001). Methane flux increased from low to intermediate Fe concentrations and declined at higher Fe levels, forming a non-monotonic response. Stratified analyses showed that this relationship was significantly stronger in the +Loach group (R^2 = 0.596, n = 76) than in the −Loach group (R^2 = 0.316, n = 76; Fig. 5). Depth-resolved patterns further indicated that the contrast was concentrated in the upper soil layer, where the Fe–CH_4 coupling was strongest in the +Loach group (R^2 = 0.751, n = 38), compared to the −Loach group (R^2 = 0.468, n = 38). In contrast, relationships in the bottom layer were weak in both

365 groups (R^2 = 0.164–0.442). Residual variance differed significantly among depth–group combinations, with
366 formal tests indicating heteroscedasticity (Bartlett test: $p = 4.1 \times 10^{-4}$; Levene test: $p = 0.013$; Fig. S6). Despite
367 this variance structure, the nonlinear Fe–CH_4 relationship and its stratified contrasts across groups and soil
368 layers remained consistent.

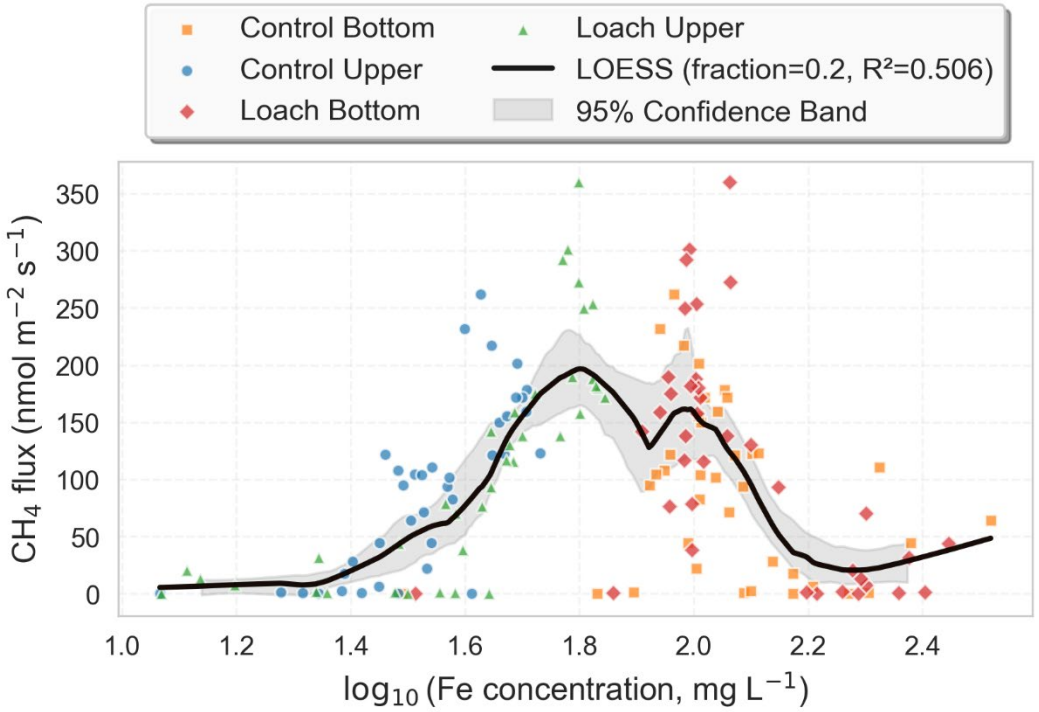

369

370 **Fig. 4. Nonlinear relationships between dissolved Fe and CH_4 dynamics across treatments and soil layers.**
371 Nonlinear relationships between CH_4 flux and dissolved Fe concentration across treatments and soil layers,
372 quantified using LOESS smoothing (fraction = 0.2). Points represent individual measurements from control and
373 loach treatments in upper and bottom soil layers (n = 120). The solid curve shows the LOESS fit, and the shaded
374 band represents the 95% bootstrap confidence interval. Residual distributions are provided to illustrate model
375 fit and variance structure. Methane flux displays a non-monotonic pattern along the dissolved Fe gradient.

376 **3.5. Process-based model simulation**

377 **(I) Iron-based model with seasonal constraint (Fe–DOY model):** The model incorporating dissolved Fe
378 dynamics and seasonal progression (DOY) captured a substantial proportion of the observed variability in CH_4
379 fluxes, supporting dissolved Fe as a key predictor of CH_4 emissions across treatments. The Fe–DOY model
380 explained a substantial proportion of the observed variability in CH_4 fluxes in both treatments, with higher
381 predictive accuracy in the −Loach group than in the +Loach group. In the −Loach group, model performance

382 reached R^2 = 0.816 and RMSE = 31.7 nmol m^{-2} s^{-1} (MAE = 24.3 nmol m^{-2} s^{-1}, NSE = 0.816; n = 38), and
383 predicted fluxes closely matched observed seasonal dynamics and cumulative emissions (Fig. 5a–b).

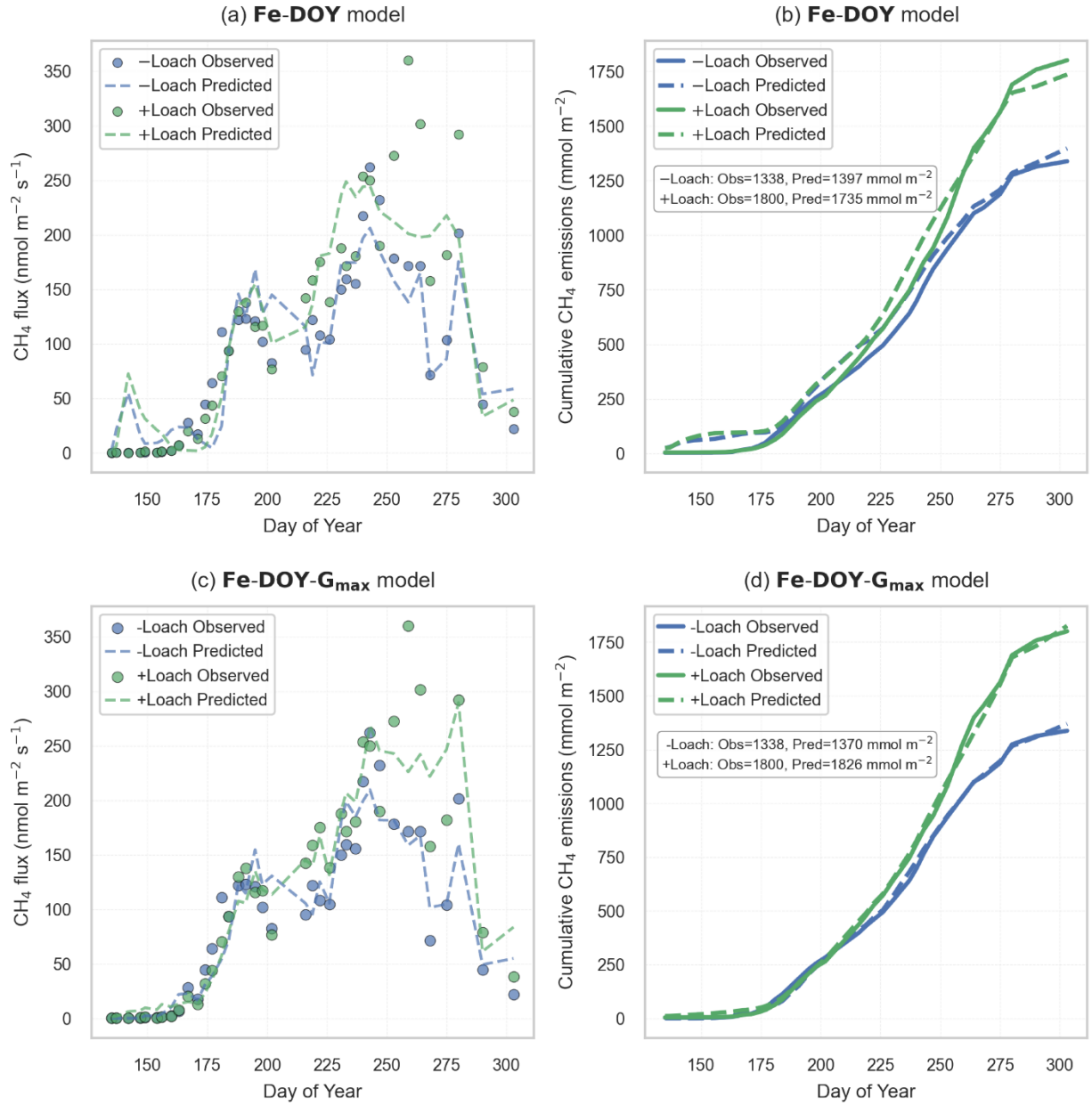

384

385 **Fig. 5. Performance of Fe-DOY and Fe-DOY-G_{max} models in predicting CH_4 emissions from paddy fields with**
386 **and without loach.** (a, b) Fe-DOY model: (a) Time series of observed and predicted CH_4 fluxes, and (b)
387 cumulative CH_4 emissions for both treatments. (c, d) Enhanced Fe-DOY-G_{max} model: (c) Time series
388 predictions incorporating photosynthetic carbon inputs with optimized lag effects, and (d) cumulative
389 emissions.

In the +Loach group, Fe–DOY model performance was lower, with R^2 = 0.783 and RMSE = 46.5 nmol m^{-2} s^{-1} (MAE = 33.2 nmol m^{-2} s^{-1}, n = 38). Underestimation was most pronounced during high-emission periods (Fig. 5a), leading to increased residual variance around peak fluxes (Fig. 5a–b). Fitted parameters differed substantially between treatments: G_{max} declined from 1000 (i.e., upper boundary with high uncertainty) to 335 nmol m^{-2} s^{-1} (−66.5%), the Fe-response exponent *m* decreased from 8.88 to 1.21 (−86.4%), and K_{emit} increased from 34.4 to 49.7 (+44.4%) in the +Loach group. Model response curve suggested that +Loach increased the CH_4 production potential ($\Psi\left(Fe^{2+}_{deep}\right)$, Eq. 2; Fig. 6) and decreased the CH_4 oxidation efficiency at the surface soil layer ($\eta\left(Fe^{2+}_{surf}\right)$, Eq. 3, Fig. 6).

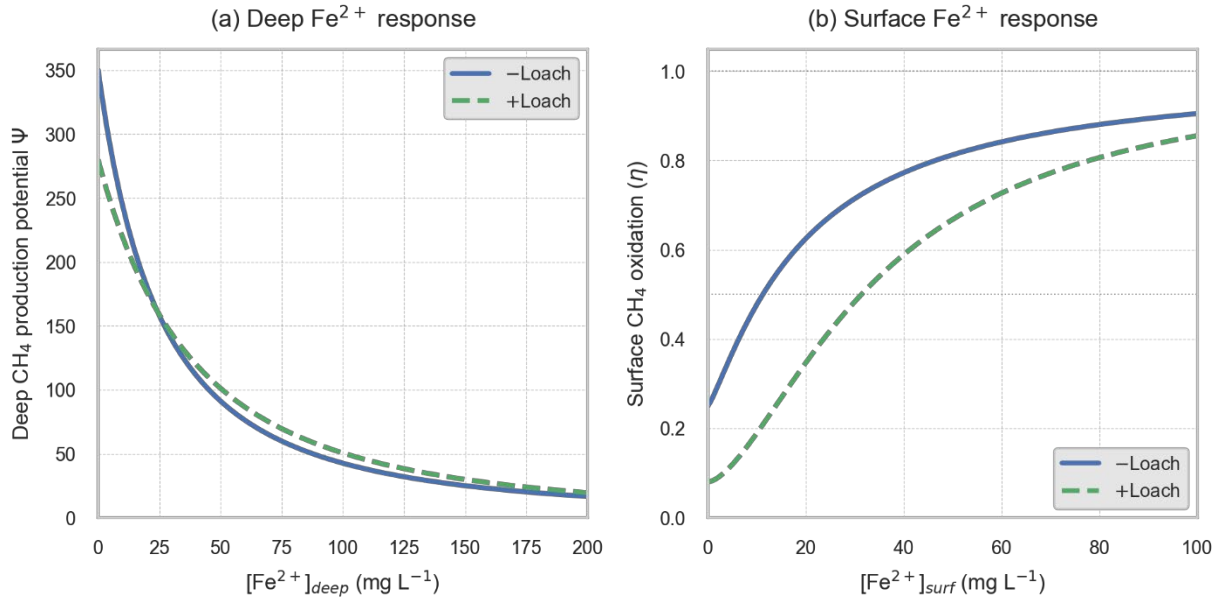

Fig. 6. Modeled CH_4 responses to dissolved Fe concentrations by Fe-DOY model. (a) Deep-layer Fe inhibits CH_4 production (Ψ) in reduced soils. (b) Surface-layer Fe promotes CH_4 oxidation (η) in oxic layers. Note: Total dissolved Fe used as proxy for Fe^{2+}.

(ii) Incorporating variable CH_4 production capacity ($Fe - DOY - G_{max}$ model, optimized parameters in Table S2): Allowing CH_4 production capacity to vary in the Fe–DOY–G_{max} model substantially improved predictive performance in both treatments (Fig. 5c, d). In the −Loach group, R^2 increased from 0.816 to 0.890 and RMSE declined from 31.7 to 24.5 nmol m^{-2} s^{-1}, while in the +Loach group, R^2 increased from 0.783 to 0.886 with RMSE reduced by 27.6%. Beyond improved goodness-of-fit metrics, the variable-G_{max} formulation enhanced model performance across the full CH_4 flux range, yielding more evenly distributed residuals (percentage of |residuals| < 1σ: 97.4%).

Plant productivity (net CO_2 flux proxy) shows a positive but lagged relationship with CH_4 emissions (Fig. S3a–b). Lag optimization further improved model fit, with optimal lags of 14 days in the −Loach group and 4 days in the +Loach group (Fig. S10, S11). The substantially shorter lag in the +Loach treatment indicates a faster coupling between recent carbon inputs and CH_4 emissions. Incorporation of treatment-specific lags reduced RMSE by 22.8% and 27.5% relative to the Fe–DOY model in the −Loach and +Loach groups, respectively, resulting in comparable predictive performance between treatments ($\Delta R^2 < 0.01$).

$\mathrm{Fe} - \mathrm{DOY} - G_{max}$ model considering the carbon-source-partitioning, plant-derived CH_4 tracked CO_2 uptake, whereas feces-derived CH_4 followed a temperature-modulated decomposition function, indicating that loach introduction substantially shifted carbon-cycling pathways. Parameter estimates revealed distinct carbon-processing pathways between treatments. In +Loach, plant-derived CH_4 capacity (G_{max}-base = 136.39 i.e., -Loach, Base maximum CH_4 production rate (nmol m^{-2} s^{-1})) was an order of magnitude lower than in −Loach, while feces-derived carbon contributed ~42% of total methanogenic potential. The Fe^{2+} trigger threshold reached the upper bound in +Loach but remained within the observed range in −Loach. In addition, model results suggested a higher temperature sensitivity of methanogenesis under +Loach conditions, as reflected by a higher Q_{10} (1.68 vs. 1.50).

4. Discussion

4.1. Does fish–rice cocultivation increase or reduce CH_4 emissions?

In this work, we evaluated the effects of loach bioturbation on CH_4 emissions in ratoon rice systems by combining long-term porewater Fe monitoring with a mechanistic modeling framework. Under continuously flooded conditions, moderate-to-high bioturbation intensity, and in the absence of external feed inputs, the presence of loach increased seasonal cumulative CH_4 emissions by 31.9% relative to rice-only controls. This magnitude is comparable to reported increases in other fish–rice systems under controlled conditions, including 27.1% in carp-based systems and 13.1% in carp–tilapia cocultivation [20, 21]. However, bioturbation altered emission magnitude but not the seasonal pattern: Peak fluxes were observed in late rice-growing stages (also see ref [21]).

Although our findings align with prior observations that ratoon rice can emit substantial higher CH_4 gas [42-44], most field-based studies supported a low-emission pattern during ratooning stage [45, 46]. These discrepancies are largely attributed by field water and straw residual management: sustained flooding and straw-returns can result high emissions (as this study did) while most low-emission cases commonly perform intermittent drainage practices for ratoon cropping [44, 46]. Sufficient evidence have demonstrated that

water-saving practice can reduce seasonal CH_4 emissions by increasing soil redox status to inhibit methanogenesis [47]. The seasonal pattern was rice growth stage-dependent in our study, which was also widely support by field observations (such as global FLUX-NET dataset [40]) or control experiments [20, 21].

In most cases, rice plants dominate terminal CH_4 emissions through plant-mediated transport, a process that is spatially and temporally decoupled from in situ methanogenesis [5, 18]. Within this conceptual context, model results further indicated that loach presence increased temperature sensitivity (Q_{10} from 1.50 to 1.68) for methanogenesis (Table S2). Under global warming scenarios, static greenhouse gas emissions from rice paddies are commonly attributed to the activities of CH_4-producing and CH_4-oxidizing microorganisms and are often assumed to be intrinsically temperature-regulated. A prevailing view holds that methanogenesis exhibits higher temperature sensitivity than CH_4 oxidation (e.g., Q10 4.1 versus 1.1), implying increased future emission risks under warming [16]. Accordingly, the net bioturbation effect on CH_4 emissions depends on whether loach activity enhances CH_4 production, for example by increasing labile carbon availability, while simultaneously reducing CH_4 oxidation through accelerated diffusion or suppression of CH_4 oxidizers at the soil–water interface and in the rhizosphere during key growth stages.

4.2. Conceptual model of loach's mechanisms on CH_4 emissions

Mechanistically, the enhancement of CH_4 emissions under loach cultivation can be primarily attributed to enhanced CH_4 production in deep soil layers and bioturbation-driven weakening of redox stratification at the SWI (Fig. 6, 7), as supported by many studies [3, 22, 48]. This is directly supported by the Fe redox chemistry (i.e., the significant difference of dissolved Fe concentrations in surface soils, Fig. 3) in this study. We also observed severe turbid of surface water frequently and that there were no clear color gradients (only consistent grey and rotted egg smells implying sulfides) of soil profile in +Loach soils.

The SWI typically acts as an oxidative barrier, oxidizing a large fraction of upward-diffusing CH_4 before it reaches the water column [3]. Repeated sediment disturbance and grazing on oxygen-producing weeds reduced the thickness and persistence of the oxic–anoxic transition zone, thereby shortening CH_4 residence time within oxidative layers and increasing the fraction of CH_4 transferred across the SWI [22, 48]. Our Fe-DOY models directly support this claim (Fig. 6). Also, as indicated by CO_2-CH_4 lags (Fig. S10, S11), bioturbation accelerates organic matter turnover through sediment resuspension, grazing on oxygen-producing weeds, and redistribution of labile carbon substrates [48, 49]. Although intense disturbance could theoretically enhance sediment oxygenation and suppress methanogenesis, such conditions were not evident in this study, consistent with moderate-to-high bioturbation intensities typical of field management [8, 22, 50]. In addition, underestimation of peak CH_4 fluxes by the Fe–DOY–G_{max} model in the +Loach treatment implies

that loach-specific mechanisms, especially physically assisted CH_4 transport, were not fully captured. Concurrent empirical observations of denser root systems in surface water and soils further suggest enhanced plant-mediated CH_4 transport contributing to elevated emissions.

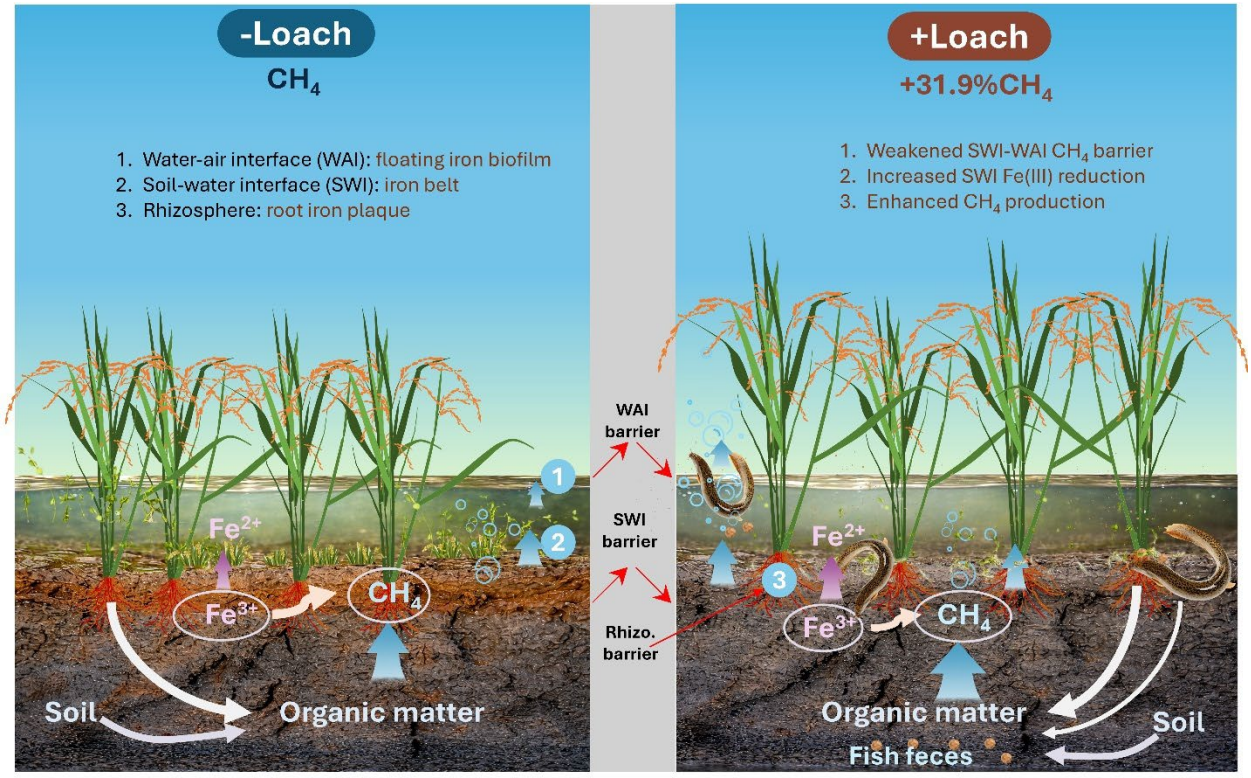

Fig. 7. Conceptual model illustrating stage-dependent pathways through which loach-mediated bioturbation regulates CH_4 emissions in rice systems. Sustained loach activity, including grazing on aquatic weeds and physical disturbance of soil surface, disrupts the SWI barrier, thereby accelerating the release of dissolved CH_4 from underlying anoxic layers. Bioturbation also promotes redox transitions among soil particles, enhancing nutrient cycling and rice growth. This leads to two major downstream consequences: (i) increased allocation of photosynthetically fixed carbon to the rhizosphere, and (ii) denser root systems that enhance deep CH_4 transport to the atmosphere. In parallel, accumulation of reduced carbon in surface soils, derived from loach feces and root exudates, further promotes Fe reduction and surface methanogenesis.

4.3. Limitations and future research priorities

Despite providing long-term porewater Fe data and a mechanistic model linking loach activity to CH_4 emissions, several limitations remain: First, key parameters in the model (e.g., CH_4 production potential, Fe reduction rate and loach-enhanced transport and oxidation were derived primarily from numerical optimization rather than independent experimental validation, introducing potential uncertainty. Second, gas

transport and oxidation processes were simplified without differentiating bubble-mediated versus diffusive pathways or surface versus rhizosphere oxidation, which may affect fine-scale interpretation of flux mechanisms. Furthermore, the study is based on a single site and a single growing season. Hydrology, fertilization, and temperature gradients in other systems may modulate the outcomes differently. Therefore, extrapolating these results to other paddy systems should be done cautiously. Future work should involve multi-site, multi-season field experiments across soils with varying Fe content and hydrological regimes, coupled with high-temporal-resolution CH_4 flux, porewater chemistry, and microbial functional data, to validate and extend the proposed mechanistic framework.

5. Conclusion

This study establishes surface-layer dissolved Fe as a practical and mechanistically grounded proxy for CH_4 emissions in flooded rice systems under sustained bioturbation. Depth-resolved microdialysis and process-based modeling show that surface dissolved Fe captures the integrity of the SWI as an oxidative barrier, which ultimately controls the fraction of methane emitted to the atmosphere. An Fe-based model alone explained >78% of seasonal CH_4 variability, outperforming bulk redox indicators and obviating reliance on episodic flux measurements. By integrating cumulative redox disturbance, carbon turnover, and transport processes, surface dissolved Fe provides a scalable alternative for estimating CH_4 emissions and offers a tractable pathway for improving methane representation in wetland and rice-paddy models.

Supplementary information

It accompanies this paper at xxx.

Author contributions

Qianrui Huangfu: Investigation, Data curation, Writing – review & editing. Sha Zhang: Project administration, Conceptualization, Methodology, Investigation, Formal analysis, Visualization, Writing – original draft, Writing – review & editing. Zheng Chen: Funding acquisition. Lu Wang: Funding acquisition. Dong Zhu: Writing – review & editing.

Data availability

The data that supports the findings of this study are available from the corresponding author upon reasonable request.

Funding

This work was supported by the National Science Foundation of China (Nos. 42595623 and 42477116).

Declarations

Competing interests

The authors declare that they have no conflict of interest.

References

[1] P.G. Falkowski, T. Fenchel, E.F. Delong, The microbial engines that drive Earth's biogeochemical cycles, Science 320(5879) (2008) 1034-9. https://doi.org/10.1126/science.1153213.

[2] R.A. Berner, The long-term carbon cycle, fossil fuels and atmospheric composition, Nature 426(6964) (2003) 323-326. https://doi.org/10.1038/nature02131.

[3] S. Zhang, Q. Huangfu, D. Zhu, Z. Chen, Floating iron biofilms as hidden barriers to methane emissions in wetlands, Innov. Geosci. 3(4) (2025) 100161-100161. https://doi.org/10.59717/j.xinn-geo.2025.100161.

[4] S. van de Velde, F.J.R. Meysman, The influence of bioturbation on iron and sulphur cycling in marine sediments: A model analysis, Aquatic Geochemistry 22(5) (2016) 469-504. https://doi.org/10.1007/s10498-016-9301-7.

[5] K. Xie, M. Wang, X. Wang, F. Li, C. Xu, J. Feng, F. Fang, Effect of rice cultivar on greenhouse-gas emissions from rice–fish co-culture, The Crop Journal 12(3) (2024) 888-896. https://doi.org/10.1016/j.cj.2024.04.011.

[6] M. Saunois, A. Martinez, B. Poulter, Z. Zhang, P. Raymond, P. Regnier, J.G. Canadell, R.B. Jackson, P.K. Patra, P. Bousquet, Global Methane Budget 2000–2020, Earth System Science Data Discussions 2024 (2024) 1-147. https://doi.org/10.5194/essd-17-1873-2025.

[7] K. Butterbach-Bahl, Papen, H. and Rennenberg, H., Impact of gas transport through rice cultivars on methane emission from rice paddy fields, Plant, Cell & Environment 20(9) (1997) 1175-1183. https://doi.org/10.1046/j.1365-3040.1997.d01-142.x.

[8] D.D.H. Fan, L. L.; Zhao, L. F.; He, L.; Tang, J. J.; Chen, X., Methane emission and the effecting factors in rice-fish system, Journal of Agro-Environment Science 44(2) (2025) 518–526. https://doi.org/10.11654/jaes.2025-0084.

[9] S. Zhang, J. Song, L. Wu, S. Du, L. Wang, D. Zhu, Z. Chen, Soil microdialysis as a tool to simulate rhizosphere dynamics and estimate metal(loid) uptake in radish (Raphanus sativus L.), Plant Soil (2025). https://doi.org/10.1007/s11104-025-07958-7.

[10] S. Zhang, Z. Yuan, Y. Cai, H. Liu, Z. Liu, Z. Chen, Dissolved solute sampling across an oxic-anoxic soil-water interface using microdialysis profilers, Journal of Visualized Experiments (193) (2023) e64358. https://doi.org/10.3791/64358.

[11] S. Zhang, Q. Huangfu, J. Boyle, L. Wu, J. Song, Z. Chen, Hotspots and dynamics of dissolved thallium species at oxic-anoxic interfaces in flooded soils, Chemosphere 377 (2025) 144331. https://doi.org/10.1016/j.chemosphere.2025.144331.

[12] G. Xu, X. Liu, Q. Wang, X. Yu, Y. Hang, Integrated rice-duck farming mitigates the global warming potential in rice season, Sci. Total Environ. 575 (2017) 58-66. https://doi.org/10.1016/j.scitotenv.2016.09.233.

[13] M. Huang, Y. Zhou, J. Guo, X. Dong, D. An, C. Shi, L. Li, Y. Dong, Q. Gao, Co-culture of rice and aquatic animals mitigates greenhouse gas emissions from rice paddies, Aquaculture International 32(2) (2024) 1785-1799. https://doi.org/10.1007/s10499-023-01243-z.

[14] E.S. Oliveira Junior, R.J.M. Temmink, B.F. Buhler, R.M. Souza, N. Resende, T. Spanings, C.C. Muniz, L.P.M. Lamers, S. Kosten, Benthivorous fish bioturbation reduces methane emissions, but increases total greenhouse gas emissions, Freshwater Biology 64(1) (2018) 197-207. https://doi.org/10.1111/fwb.13209.

[15] H.-C. Tseng, N. Fujimoto, A. Ohnishi, Biodegradability and methane fermentability of polylactic acid by thermophilic methane fermentation, Bioresource Technology Reports 8 (2019) 100327. https://doi.org/10.1016/j.biteb.2019.100327.

[16] J. Zheng, T. RoyChowdhury, Z. Yang, B. Gu, S.D. Wullschleger, D.E. Graham, Impacts of temperature and soil characteristics on methane production and oxidation in Arctic tundra, Biogeosciences 15(21) (2018) 6621-6635. https://doi.org/10.5194/bg-15-6621-2018.

[17] Q.H.X. Li, Q. Y.; Ye, P., Research on the law of greenhouse gas emissions from rice fields under the rice-shrimp planting and breeding model, Hubei Agricultural Sciences 62(10) (2023) 30-36. https://doi.org/10.14088/j.cnki.issn0439-8114.2023.10.007.

[18] L. Zhao, R. Dai, T. Zhang, L. Guo, Q. Luo, J. Chen, S. Zhu, X. Xu, J. Tang, L. Hu, X. Chen, Fish mediate surface soil methane oxidation in the agriculture heritage rice–fish system, Ecosystems 26(8) (2023) 1656-1669. https://doi.org/10.1007/s10021-023-00856-y.

[19] H.L. Fan D, Zhao L, He L, Tang J, Chen X, Methane emission and the effecting factors in rice-fish system, Journal of Agro-Environment Science 44(2) (2025) 518-526. https://doi.org/10.11654/jaes.2025-0084.

[20] A. Datta, D.R. Nayak, D.P. Sinhababu, T.K. Adhya, Methane and nitrous oxide emissions from an integrated rainfed rice–fish farming system of Eastern India, Agriculture, Ecosystems & Environment 129(1) (2009) 228-237. https://doi.org/https://doi.org/10.1016/j.agee.2008.09.003.

[21] M. Frei, K. Becker, Integrated rice–fish production and methane emission under greenhouse conditions, Agriculture, Ecosystems & Environment 107(1) (2005) 51-56. https://doi.org/10.1016/j.agee.2004.10.026.

[22] M.T. Booth, M. Urbanic, X. Wang, J.J. Beaulieu, Bioturbation frequency alters methane emissions from reservoir sediments, Sci. Total Environ. 789 (2021) 148033. https://doi.org/https://doi.org/10.1016/j.scitotenv.2021.148033.

[23] Z. Zhong, Y. Ruan, J. Qian, M. Xie, Q.-G. Tan, R. Chen, Paphia undulata enhances sedimentary CH_4 and N_2O emissions via divergent microbial mechanisms, Available at SSRN 6087164 (2026). https://doi.org/10.2139/ssrn.6087164.

[24] M. Wang, F. Li, J. Wu, T. Yang, C. Xu, L. Zhao, Y. Liu, F. Fang, J. Feng, Response of CH_4 and N_2O emissions to the feeding rates in a pond rice-fish co-culture system, Environmental Science and Pollution Research 31(40) (2024) 53437-53446. https://doi.org/10.1007/s11356-024-34772-y.

[25] S.L. D'Ambrosio, J.A. Harrison, Measuring CH_4 fluxes from lake and reservoir sediments: Methodologies and needs, Frontiers in Environmental Science Volume 10 - 2022 (2022). https://doi.org/10.3389/fenvs.2022.850070.

[26] P. Polsenaere, B. Deflandre, G. Thouzeau, S. Rigaud, T. Cox, E. Amice, T.L. Bec, I. Bihannic, O. Maire, Comparison of benthic oxygen exchange measured by aquatic Eddy Covariance and Benthic Chambers in two contrasting coastal biotopes (Bay of Brest, France), Regional Studies in Marine Science 43 (2021) 101668. https://doi.org/10.1016/j.rsma.2021.101668.

[27] Q. Huangfu, S. Zhang, Y. Guo, L. Wang, Z. Chen, S. Du, Elevated soil temperatures during a heatwave year do not necessarily increase metal(loid) mobilization or accumulation across two harvests of semi-perennial rice: evidence from mesocosm experiments, Environmental and Biogeochemical Processes 1(1) (2025). https://doi.org/10.48130/ebp-0025-0017.

[28] O. Husson, Redox potential (Eh) and pH as drivers of soil/plant/microorganism systems: a transdisciplinary overview pointing to integrative opportunities for agronomy, Plant Soil 362(1) (2013) 389-417. https://doi.org/10.1007/s11104-012-1429-7.

[29] N. Riedinger, M.J. Formolo, T.W. Lyons, S. Henkel, A. Beck, S. Kasten, An inorganic geochemical argument for coupled anaerobic oxidation of methane and iron reduction in marine sediments, Geobiology 12(2) (2014) 172-181. https://doi.org/10.1111/gbi.12077.

[30] T. Fumoto, Process-based modeling of methane emissions from rice fields, Bulletin of the NARO, Agro-Environmental Sciences (38) (2017). https://doi.org/https://www.naro.go.jp/publicity_report/publication/files/niaes_report38-2.pdf.

[31] C. Chen, S.J. Hall, E. Coward, A. Thompson, Iron-mediated organic matter decomposition in humid soils can counteract protection, Nat. Commun. 11(1) (2020) 2255. https://doi.org/10.1038/s41467-020-16071-5.

[32] W.H. Yang, G. McNicol, Y.A. Teh, K. Estera-Molina, T.E. Wood, W.L. Silver, Evaluating the classical versus an emerging conceptual model of peatland methane dynamics, Global Biogeochem. Cycles 31(9) (2017) 1435-1453. https://doi.org/10.1002/2017GB005622.

[33] B.N. Sulman, F. Yuan, T. O'Meara, B. Gu, E.M. Herndon, J. Zheng, P.E. Thornton, D.E. Graham, Simulated hydrological dynamics and coupled iron redox cycling impact methane production in an Arctic soil, J. Geophys. Res. Biogeosci. 127(10) (2022) e2021JG006662. https://doi.org/10.1029/2021JG006662.

[34] P. van Bodegom, F. Stams, L. Mollema, S. Boeke, P. Leffelaar, Methane oxidation and the competition for oxygen in the rice rhizosphere, Appl Environ Microbiol 67(8) (2001) 3586-97. https://doi.org/10.1128/aem.67.8.3586-3597.2001.

[35] Y. Guo, S. Zhang, W. Gustave, H. Liu, Y. Cai, Y. Wei, Z. Chen, Dynamics of cadmium and arsenic at the capillary fringe of paddy soils: A microcosm study based on high-resolution porewater analysis, Soil & Environmental Health 2(1) (2024) 100057. https://doi.org/10.1016/j.seh.2023.100057.

[36] M. Ueyama, R. Takeuchi, Y. Takahashi, R. Ide, M. Ataka, Y. Kosugi, K. Takahashi, N. Saigusa, Methane uptake in a temperate forest soil using continuous closed-chamber measurements, Agric. For. Meteorol. 213 (2015) 1-9. https://doi.org/10.1016/j.agrformet.2015.05.004.

[37] O. Sivan, S.S. Shusta, D.L. Valentine, Methanogens rapidly transition from methane production to iron reduction, Geobiology 14(2) (2016) 190-203. https://doi.org/10.1111/gbi.12172.

[38] T. Borch, R. Kretzschmar, A. Kappler, P.V. Cappellen, M. Ginder-Vogel, A. Voegelin, K. Campbell, Biogeochemical redox processes and their impact on contaminant dynamics, Environ. Sci. Technol. 44(1) (2010) 15-23. https://doi.org/10.1021/es9026248.

[39] G. McNicol, E. Fluet-Chouinard, Z. Ouyang, S. Knox, Z. Zhang, T. Aalto, S. Bansal, K.-Y. Chang, M. Chen, K. Delwiche, S. Feron, M. Goeckede, J. Liu, A. Malhotra, J.R. Melton, W. Riley, R. Vargas, K. Yuan, Q. Ying, Q. Zhu, P. Alekseychik, M. Aurela, D.P. Billesbach, D.I. Campbell, J. Chen, H. Chu, A.R. Desai, E. Euskirchen, J. Goodrich, T. Griffis, M. Helbig, T. Hirano, H. Iwata, G. Jurasinski, J. King, F. Koebsch, R. Kolka, K. Krauss, A. Lohila, I. Mammarella, M. Nilson, A. Noormets, W. Oechel, M. Peichl, T. Sachs, A. Sakabe, C. Schulze, O. Sonnentag, R.C. Sullivan, E.-S. Tuittila, M. Ueyama, T. Vesala, E. Ward, C. Wille, G.X. Wong, D. Zona, L. Windham-Myers, B. Poulter, R.B. Jackson, Upscaling wetland methane emissions from the fluxnet-ch4 eddy covariance network (upch4 v1.0): model development, network assessment, and budget comparison, AGU Advances 4(5) (2023) e2023AV000956. https://doi.org/10.1029/2023AV000956.

[40] S.H. Knox, S. Bansal, G. McNicol, K. Schafer, C. Sturtevant, M. Ueyama, A.C. Valach, D. Baldocchi, K. Delwiche, A.R. Desai, E. Euskirchen, J. Liu, A. Lohila, A. Malhotra, L. Melling, W. Riley, B.R.K. Runkle, J. Turner, R. Vargas, Q. Zhu, T. Alto, E. Fluet-Chouinard, M. Goeckede, J.R. Melton, O. Sonnentag, T. Vesala, E. Ward, Z. Zhang, S. Feron, Z. Ouyang, P. Alekseychik, M. Aurela, G. Bohrer, D.I. Campbell, J. Chen, H. Chu, H.J. Dalmagro, J.P. Goodrich, P. Gottschalk, T. Hirano, H. Iwata, G. Jurasinski, M. Kang, F. Koebsch, I. Mammarella, M.B. Nilsson, K. Ono, M. Peichl, O. Peltola, Y. Ryu, T. Sachs, A. Sakabe, J.P. Sparks, E.-S. Tuittila, G.L. Vourlitis, G.X. Wong, L. Windham-Myers, B. Poulter, R.B. Jackson, Identifying dominant environmental predictors of freshwater wetland methane fluxes across diurnal to seasonal time scales, Global Change Biology 27(15) (2021) 3582-3604. https://doi.org/10.1111/gcb.15661.

[41] C. Wang, D.Y.F. Lai, C. Tong, W. Wang, J. Huang, C. Zeng, Variations in Temperature sensitivity (Q_{10}) of CH_4 emission from a subtropical estuarine marsh in southeast China, PLoS One 10(5) (2015) e0125227. https://doi.org/10.1371/journal.pone.0125227.

[42] C.W. Lindau, P. Bollich, Methane emissions from Louisiana first and ratoon crop rice, Soil Sci. 156(1) (1993) 42-48. https://doi.org/10.1097/00010694-199307000-00006.

[43] C. Lindau, P. Bollich, R. DeLaune, Effect of rice variety on methane emission from Louisiana rice, Agriculture, Ecosystems & Environment 54(1-2) (1995) 109-114. https://doi.org/10.1016/0167-8809(95)00587-I.

[44] M. Leavitt, B. Moreno-García, C.W. Reavis, M.L. Reba, B.R.K. Runkle, The effect of water management and ratoon rice cropping on methane emissions and yield in Arkansas, Agriculture, Ecosystems & Environment 356 (2023) 108652. https://doi.org/10.1016/j.agee.2023.108652.

[45] X. Ren, K. Cui, Z. Deng, K. Han, Y. Peng, J. Zhou, Z. Zhai, J. Huang, S. Peng, Ratoon rice cropping mitigates the greenhouse effect by reducing CH_4 emissions through reduction of biomass during the ratoon season, Plants (Basel) 12(19) (2023). https://doi.org/10.3390/plants12193354.

[46] Q. Ding, Y. Li, R. Cao, J. Chen, X. Yao, W. Zhang, Spatial optimization of rice systems with ratoon rice increases production and reduces methane emissions, European Journal of Agronomy 170 (2025) 127720. https://doi.org/https://doi.org/10.1016/j.eja.2025.127720.

[47] B.A. Linquist, M. Marcos, M.A. Adviento-Borbe, M. Anders, D. Harrell, S. Linscombe, M.L. Reba, B.R.K. Runkle, L. Tarpley, A. Thomson, Greenhouse gas emissions and management practices that affect emissions in US rice systems, J. Environ. Qual. 47(3) (2018) 395-409. https://doi.org/10.2134/jeq2017.11.0445.

[48] E. Broman, M. Olsson, A. Maciute, D. Donald, C. Humborg, A. Norkko, T. Jilbert, S. Bonaglia, F.J.A. Nascimento, Biotic interactions between benthic infauna and aerobic methanotrophs mediate methane fluxes from coastal sediments, ISME J. 18(1) (2024). https://doi.org/10.1093/ismejo/wrae013.

[49] L. Nie, Y. Li, Y. Hou, L. Di, M. Xi, Z. Yu, Dynamics of organic carbon under bioturbation by mud crabs (Macrophthalmus japonicus) and clamworms (Perinereis aibuhitensis) in an estuary ecosystem, Journal of Experimental Marine Biology and Ecology 534 (2021) 151474. https://doi.org/10.1016/j.jembe.2020.151474.

[50] I. Bussmann, Methane Release through Resuspension of Littoral Sediment, Biogeochemistry 74(3) (2005) 283-302. https://doi.org/10.1007/s10533-004-2223-2.

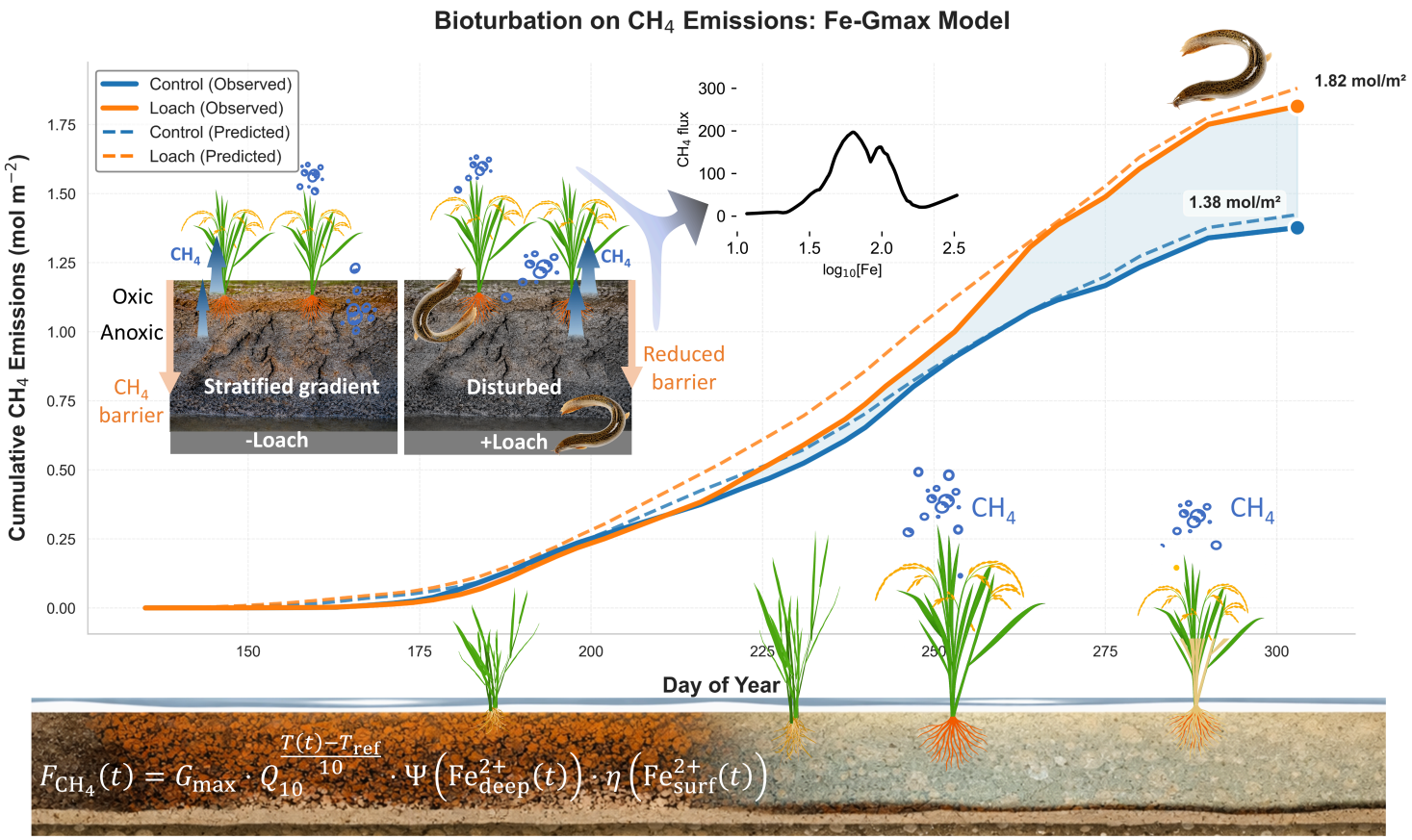
Bioturbation on CH4 Emissions: Fe-Gmax Model
Control (Observed)
Loach (Observed)
Control (Predicted)
Loach (Predicted)
Cumulative CH4 Emissions (mol m−2)
1.75
1.50
1.25
1.00
0.75
0.50
0.25
0.00
150
175
200
225
250
275
300
Day of Year
1.82 mol/m²
1.38 mol/m²
CH4 flux
300
200
100
0
1.0
1.5
2.0
2.5
log10[Fe]
CH4
Oxic
Anoxic
CH4 barrier
Stratified gradient
-Loach
Disturbed
+Loach
Reduced barrier
CH4
CH4
$F_{CH_4}(t) = G_{max} \cdot Q_{10}^{\frac{T(t)-T_{ref}}{10}} \cdot \Psi\left(Fe^{2+}_{deep}(t)\right) \cdot \eta\left(Fe^{2+}_{surf}(t)\right)$

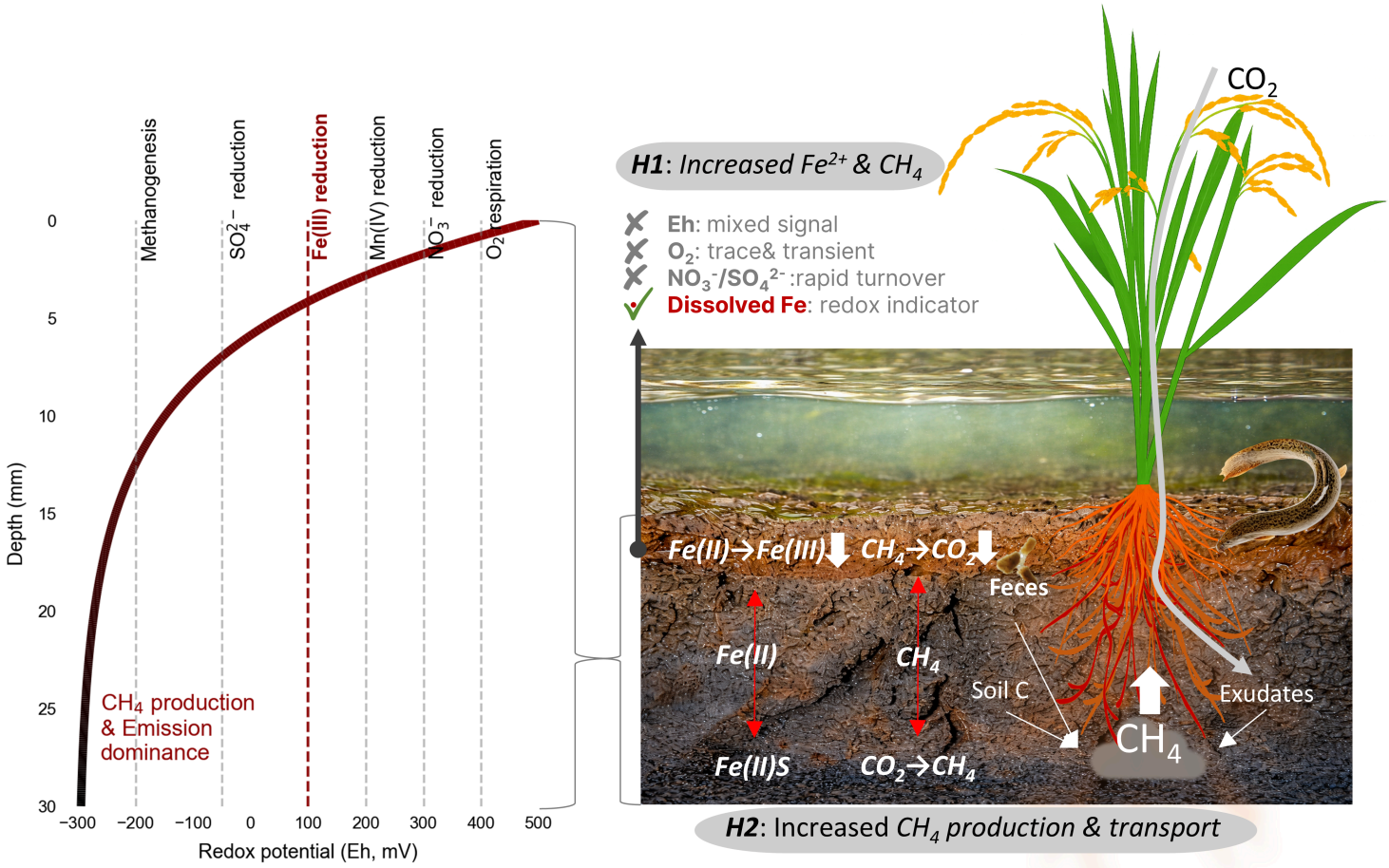
Methanogenesis
SO_4^{2-} reduction
Fe(III) reduction
Mn(IV) reduction
NO_3^- reduction
O_2 respiration
Depth (mm)
0
5
10
15
20
25
30
−300
−200
−100
0
100
200
300
400
500
Redox potential (Eh, mV)
CH_4 production & Emission dominance
H1: Increased Fe^{2+} & CH_4
Eh: mixed signal
O_2: trace& transient
NO_3^-/SO_4^{2-} :rapid turnover
Dissolved Fe: redox indicator
CO_2
Fe(II)→Fe(III)
CH_4→CO_2
Feces
Fe(II)
CH_4
Soil C
Exudates
Fe(II)S
CO_2→CH_4
CH_4
H2: Increased CH_4 production & transport

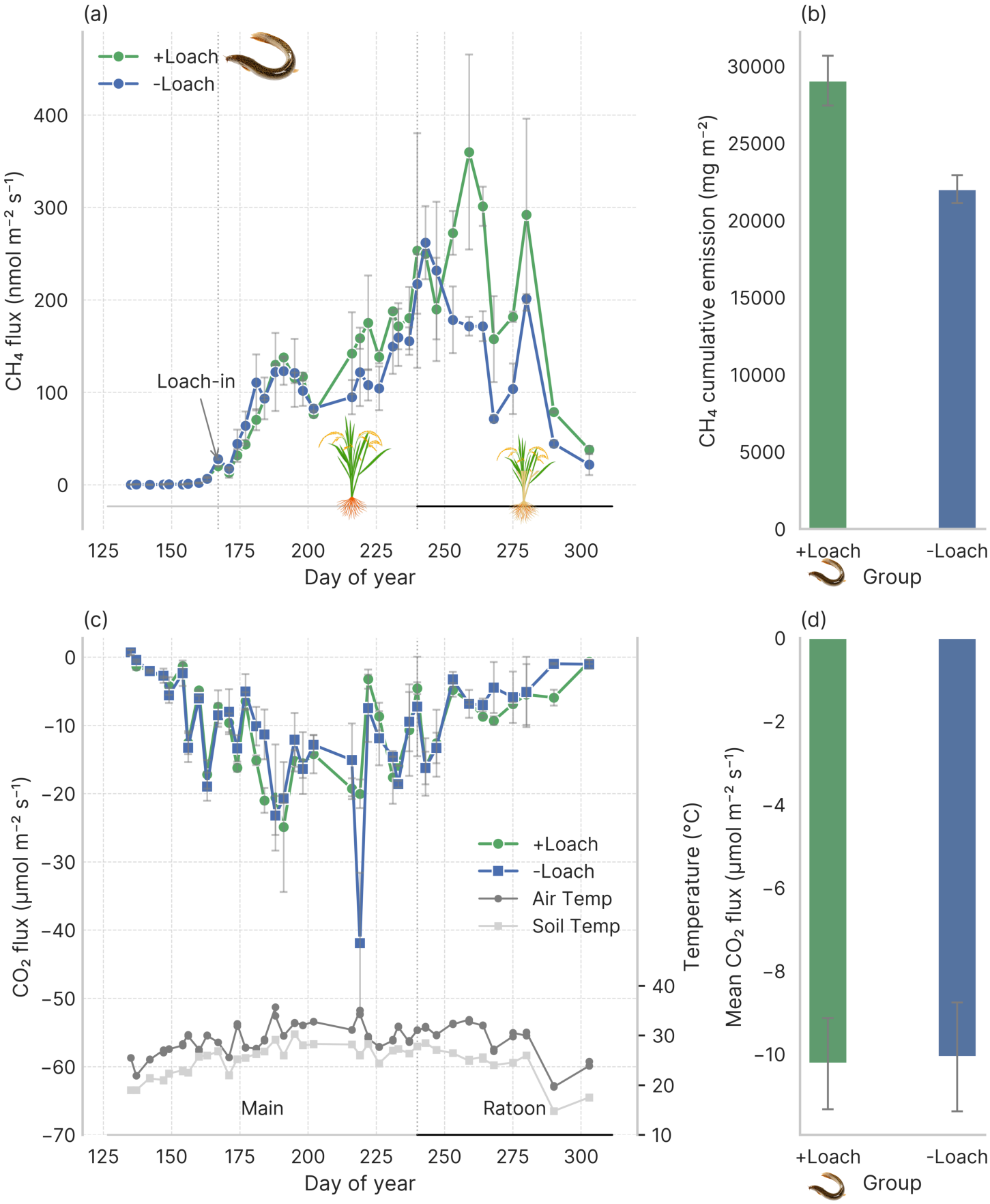
(a)
+Loach
-Loach
CH4 flux (nmol m−2 s−1)
400
300
200
100
0
Loach-in
125
150
175
200
225
250
275
300
Day of year
(b)
CH4 cumulative emission (mg m−2)
30000
25000
20000
15000
10000
5000
0
+Loach
-Loach
Group
(c)
CO2 flux (μmol m−2 s−1)
0
−10
−20
−30
−40
−50
−60
−70
+Loach
-Loach
Air Temp
Soil Temp
Temperature (°C)
40
30
20
10
Main
Ratoon
125
150
175
200
225
250
275
300
Day of year
(d)
Mean CO2 flux (μmol m−2 s−1)
0
−2
−4
−6
−8
−10
+Loach
-Loach
Group

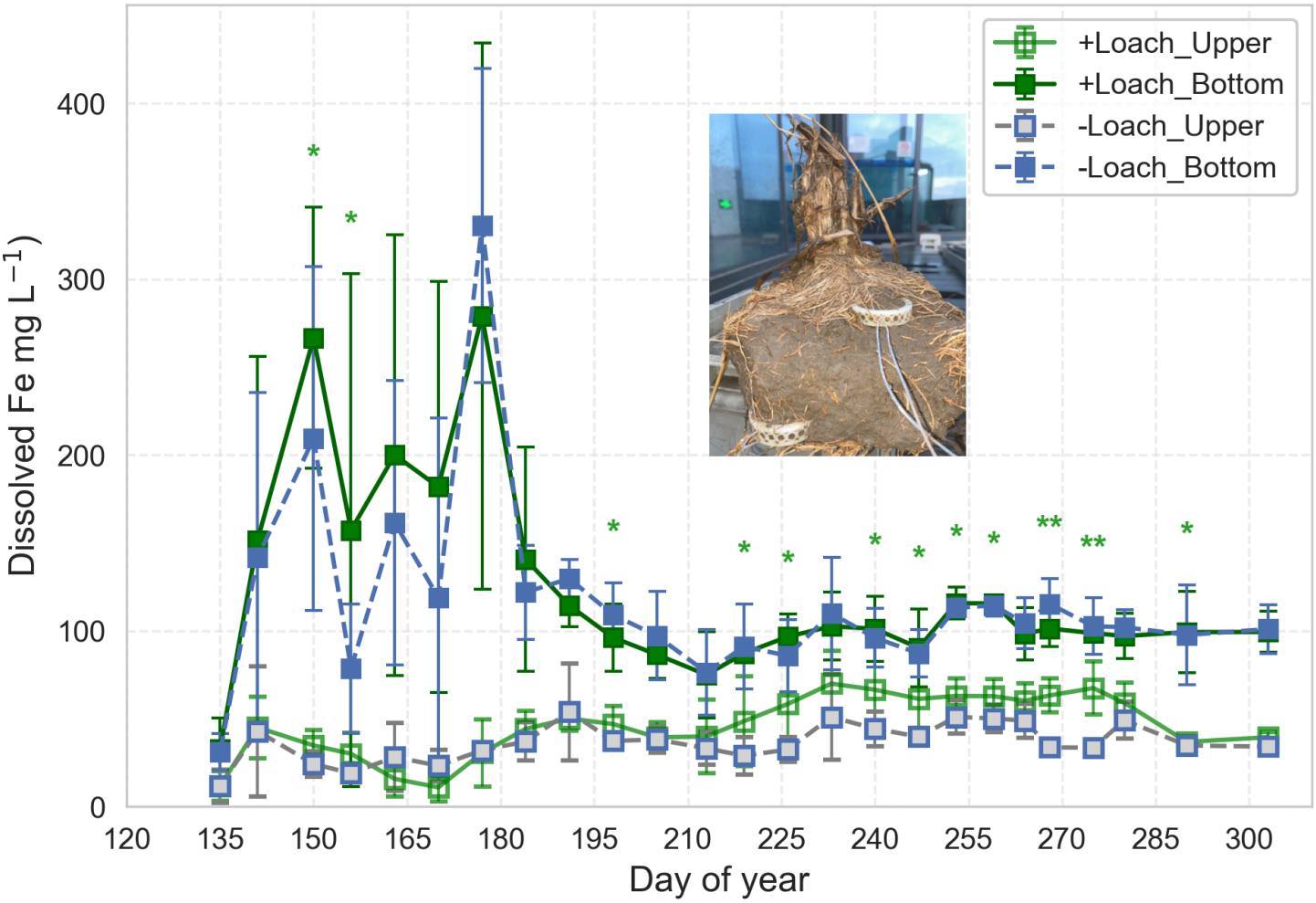
+Loach_Upper
+Loach_Bottom
-Loach_Upper
-Loach_Bottom
Dissolved Fe mg L^{-1})
Day of year
0
100
200
300
400
120
135
150
165
180
195
210
225
240
255
270
285
300
*
**

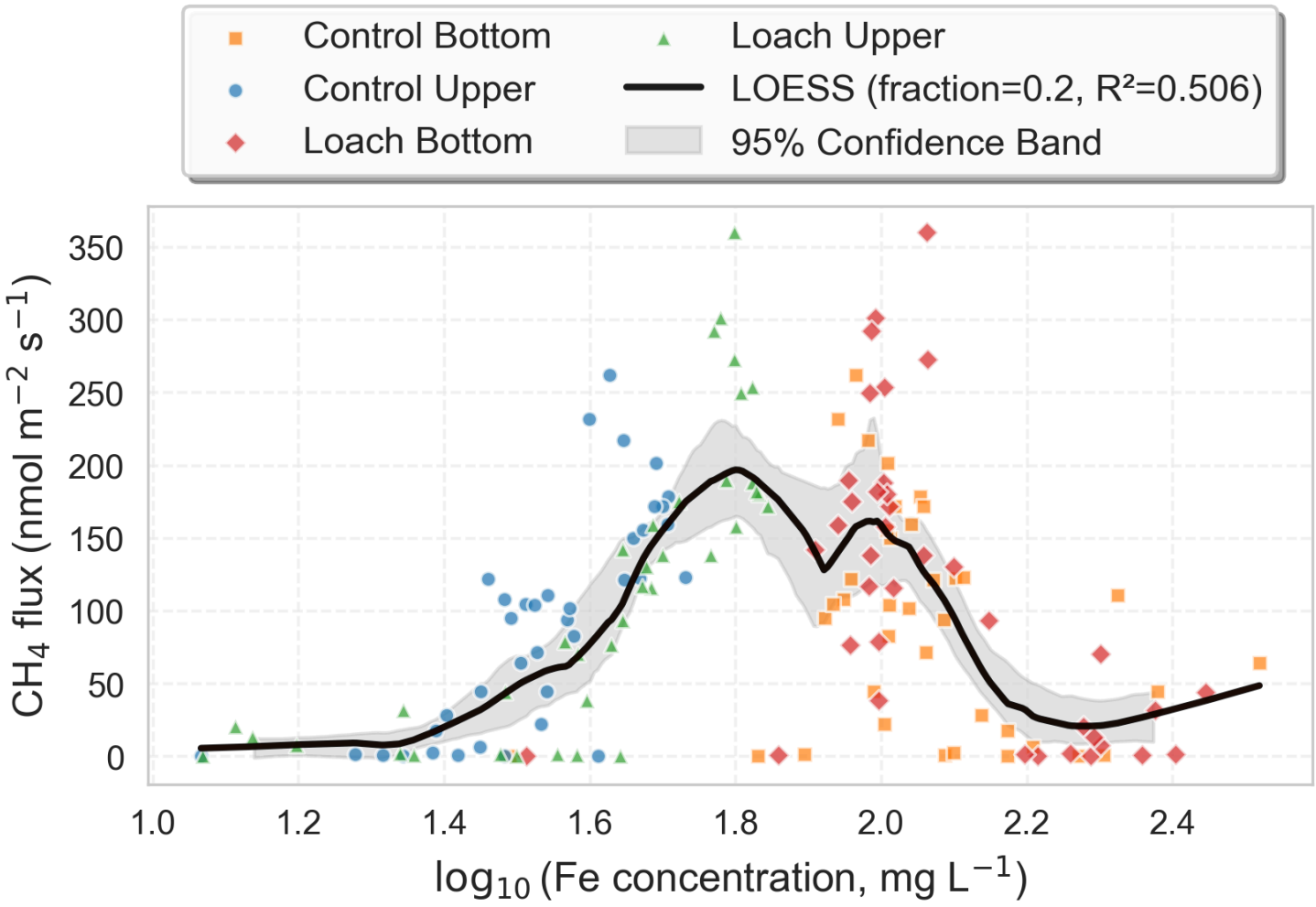
Control Bottom
Control Upper
Loach Bottom
Loach Upper
LOESS (fraction=0.2, R²=0.506)
95% Confidence Band
CH4 flux (nmol m−2 s−1)
350
300
250
200
150
100
50
0
1.0
1.2
1.4
1.6
1.8
2.0
2.2
2.4
log10 (Fe concentration, mg L−1)

(a) **Fe-DOY** model

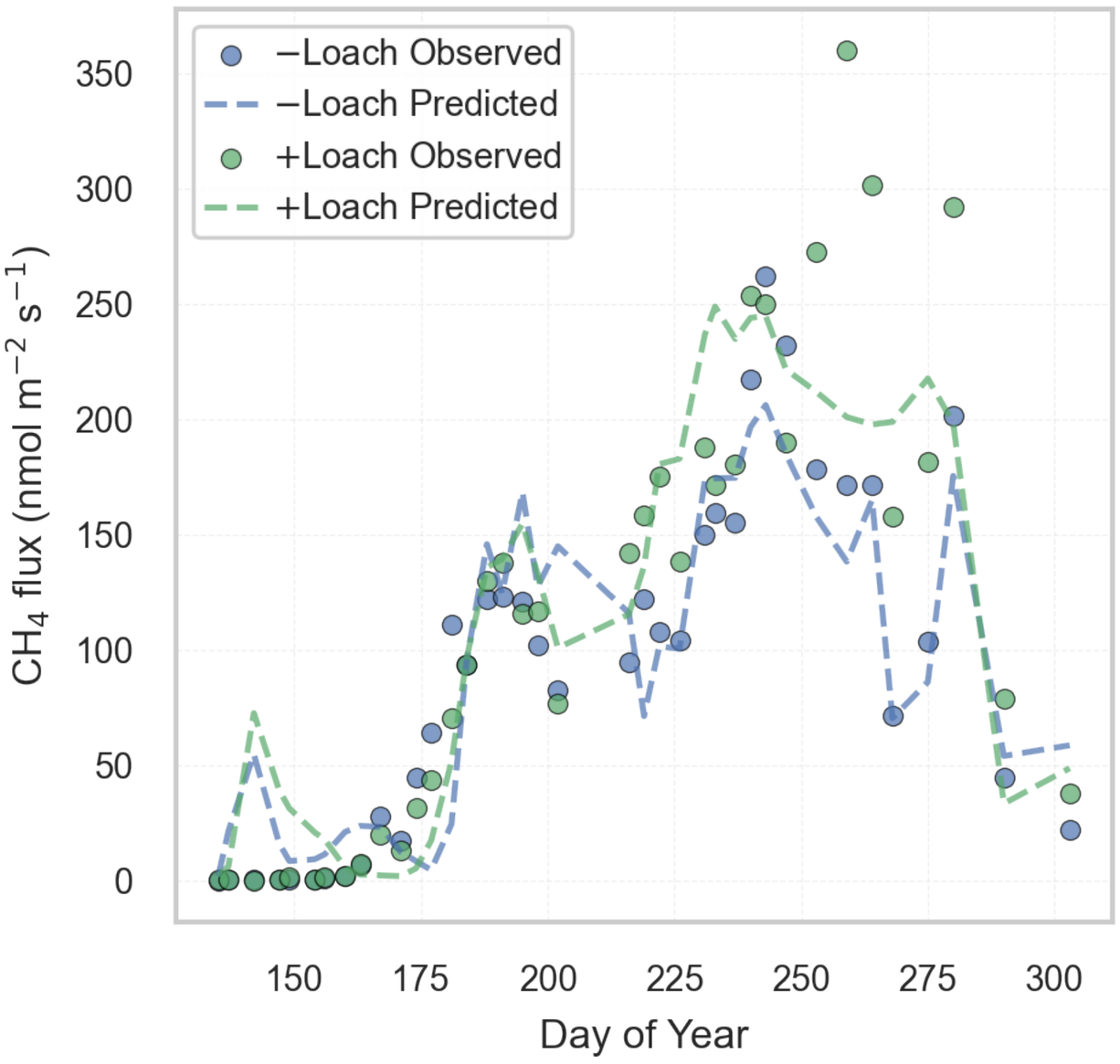

(b) **Fe-DOY** model

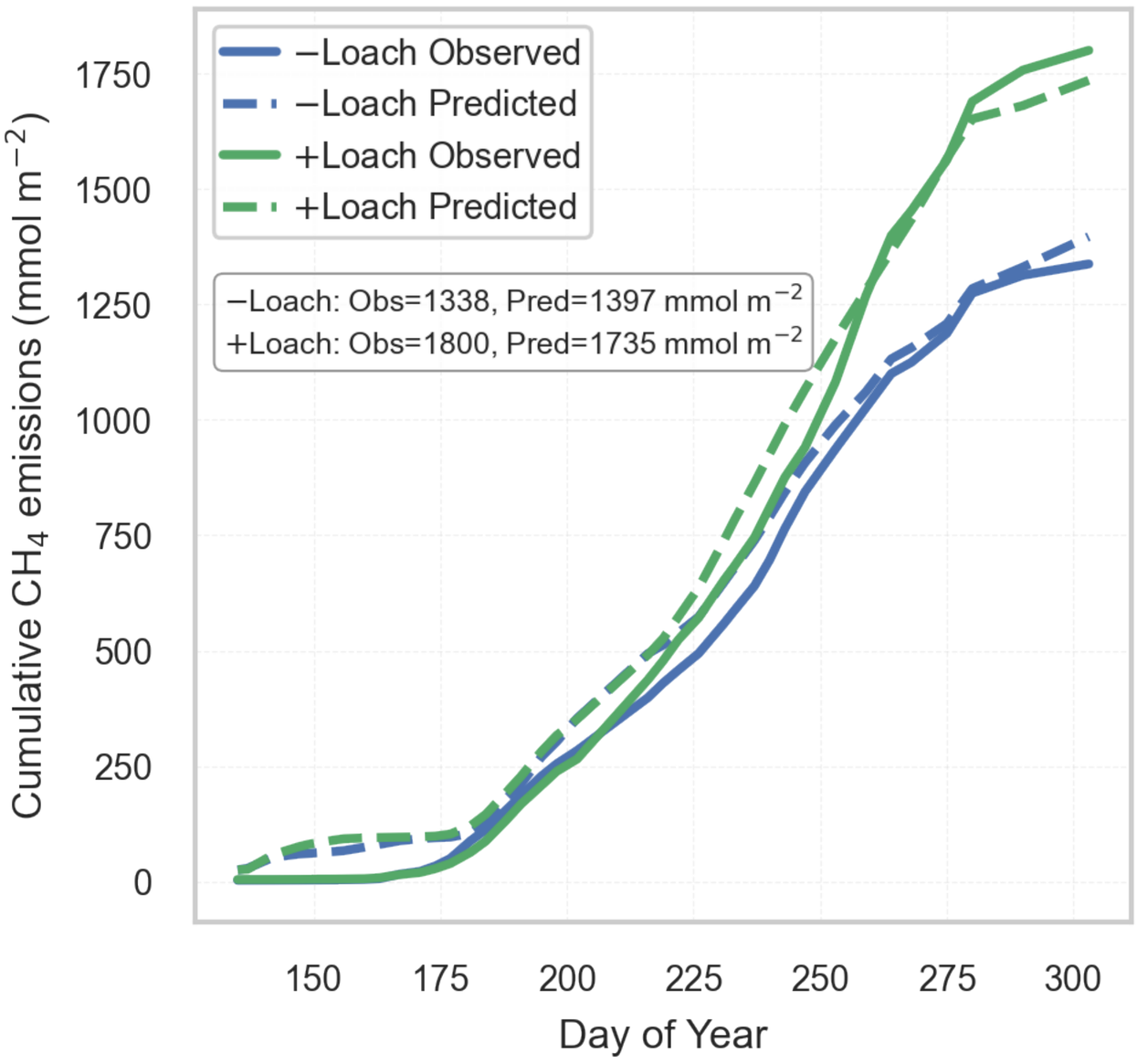

(c) **Fe-DOY-G_{max}** model

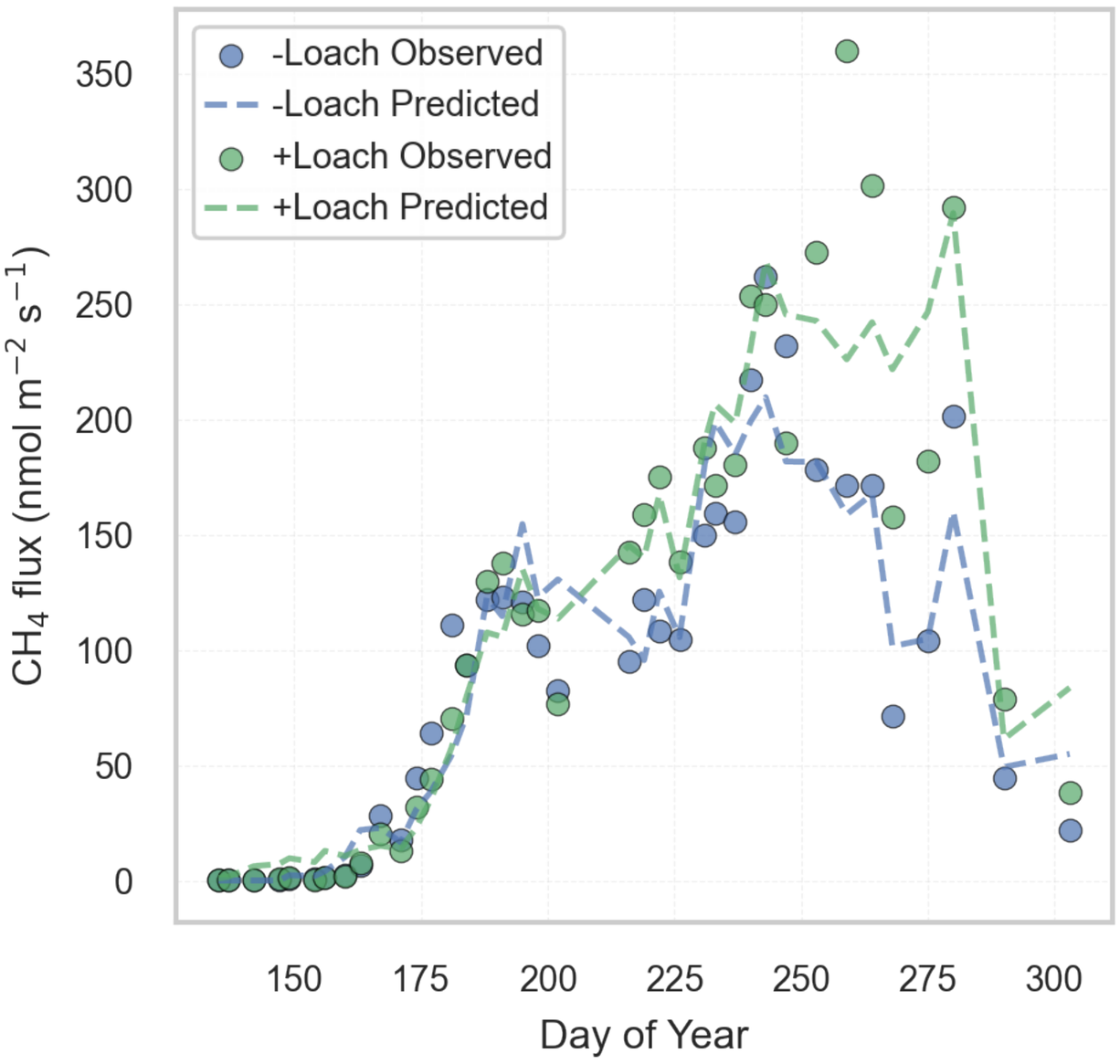

(d) **Fe-DOY-G_{max}** model

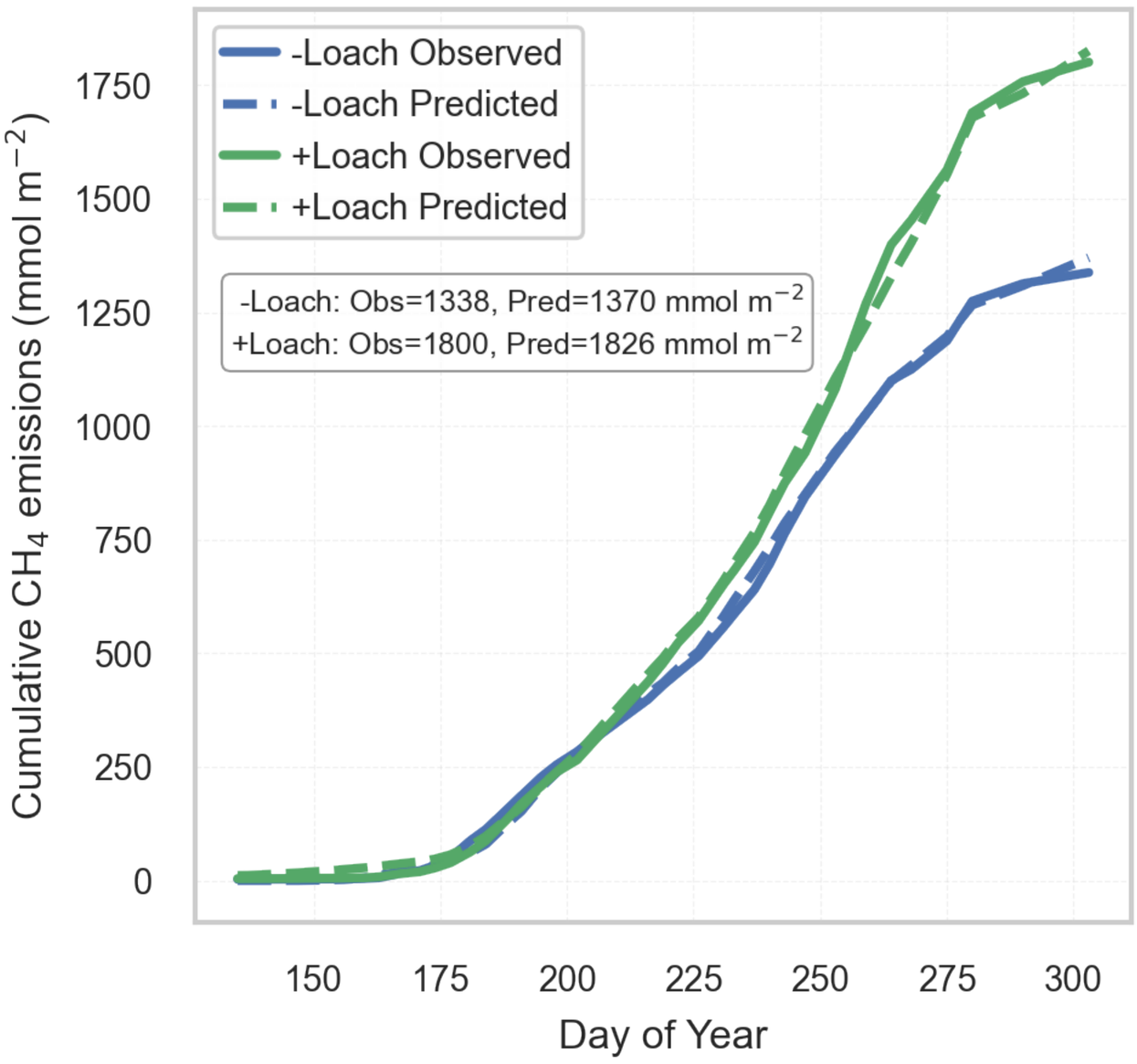

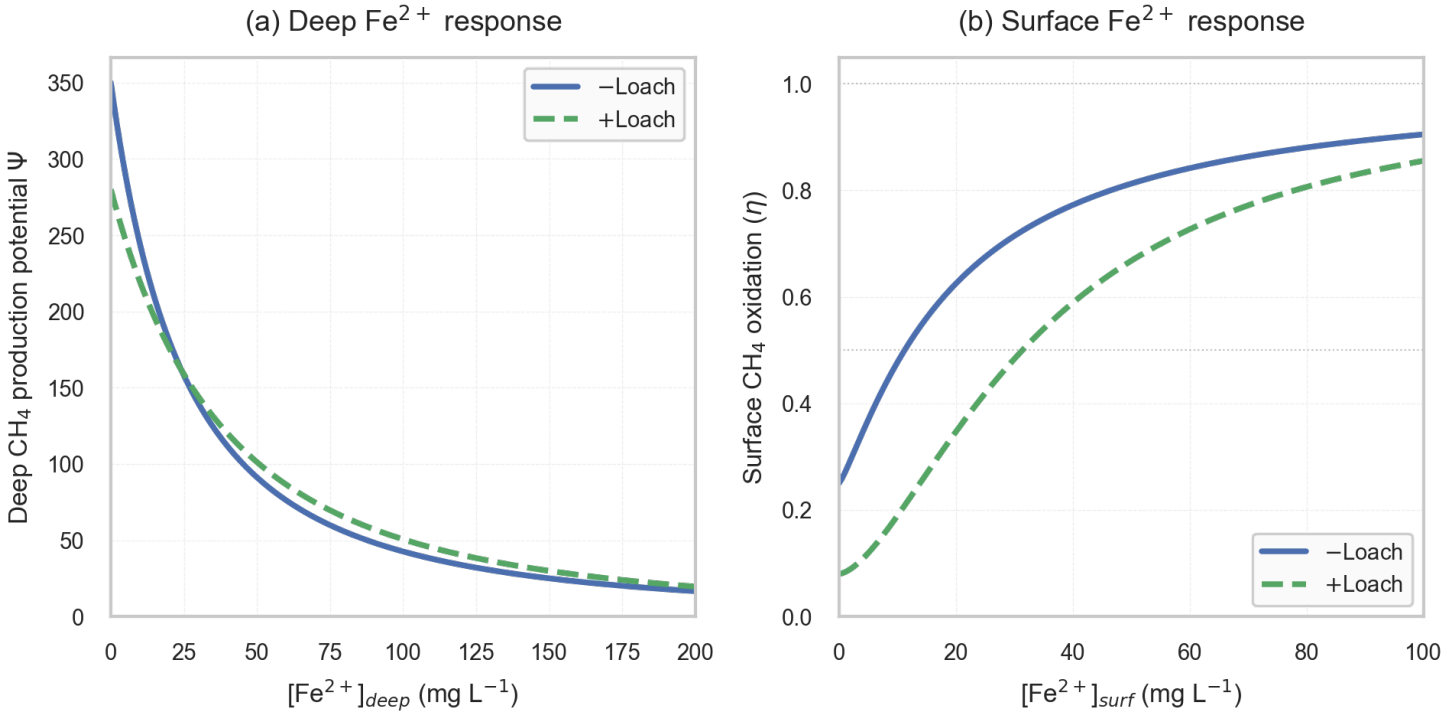
(a) Deep Fe^{2+} response
Deep CH_4 production potential Ψ
$[Fe^{2+}]_{deep}$ (mg L^{-1})
−Loach
+Loach
0
50
100
150
200
250
300
350
0
25
50
75
100
125
150
175
200
(b) Surface Fe^{2+} response
Surface CH_4 oxidation (η)
$[Fe^{2+}]_{surf}$ (mg L^{-1})
−Loach
+Loach
0.0
0.2
0.4
0.6
0.8
1.0
0
20
40
60
80
100

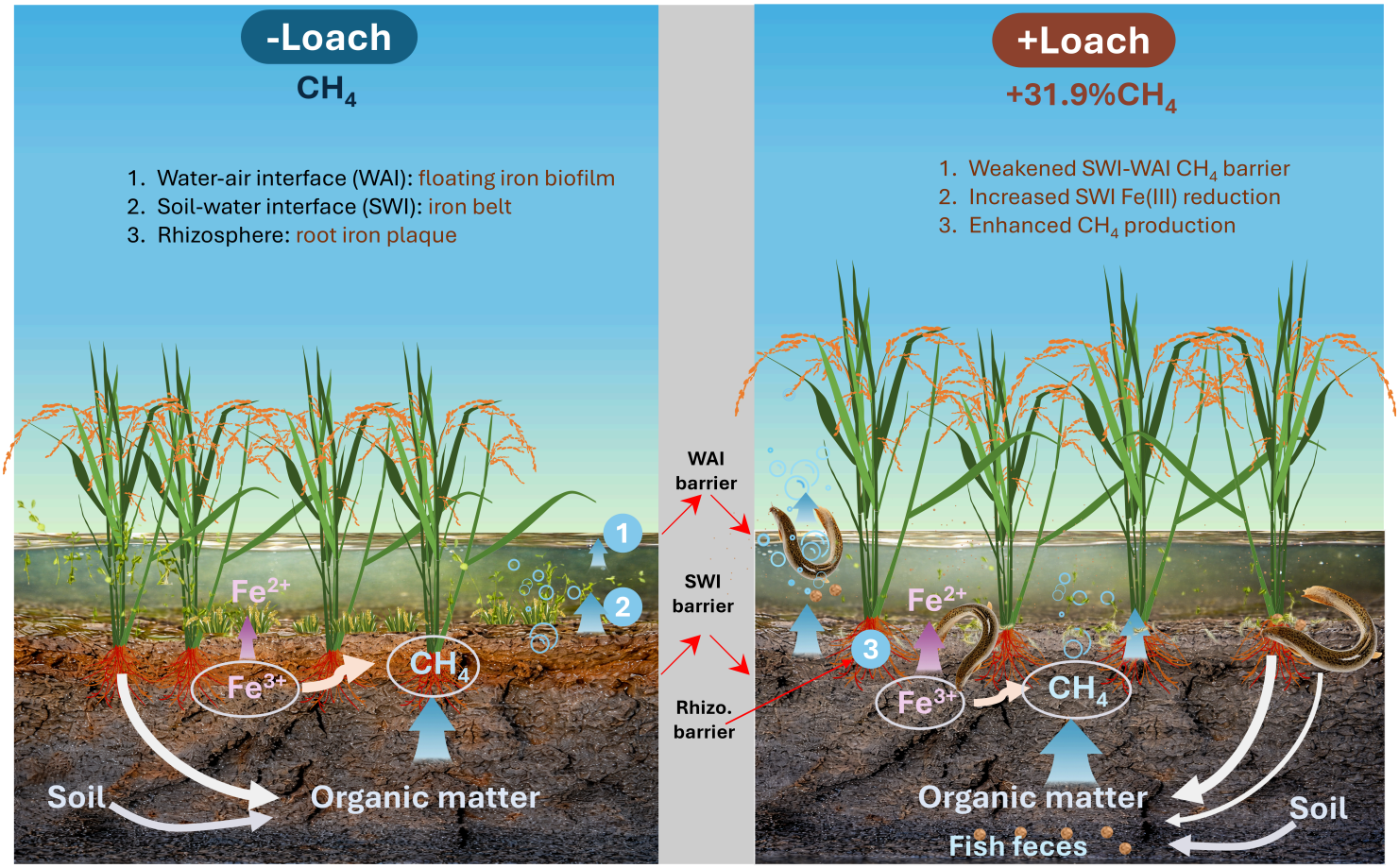
-Loach
CH4
1. Water-air interface (WAI): floating iron biofilm
2. Soil-water interface (SWI): iron belt
3. Rhizosphere: root iron plaque
Fe2+
Fe3+
CH4
1
2
Soil
Organic matter
WAI barrier
SWI barrier
Rhizo. barrier
+Loach
+31.9%CH4
1. Weakened SWI-WAI CH4 barrier
2. Increased SWI Fe(III) reduction
3. Enhanced CH4 production
3
Fe2+
Fe3+
CH4
Organic matter
Soil
Fish feces